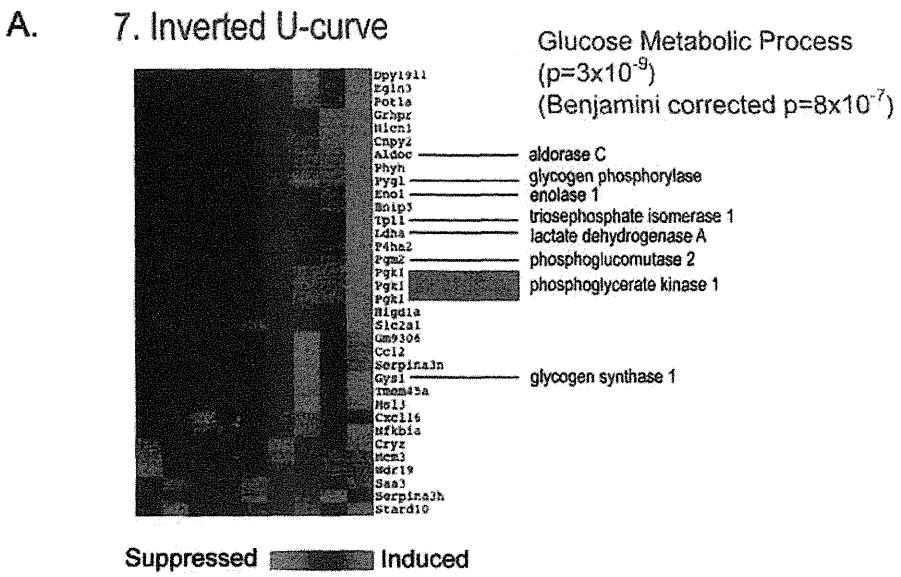

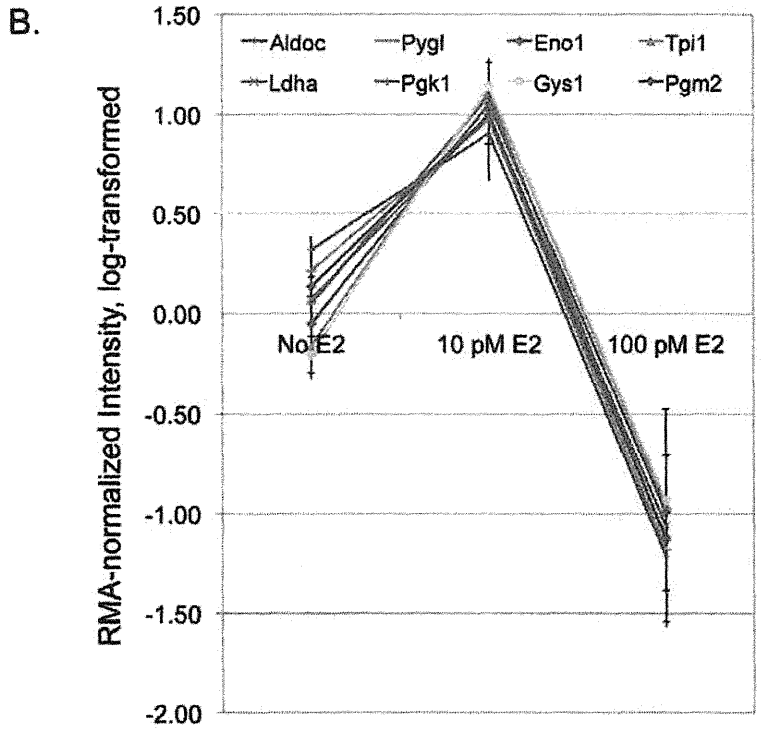

Figure 4. Detail of E2-suppressible genes in groups separated by clustering analysis. A) Set 7: Inverted U-curve. Both raw p values and Benjamini-Hochberg corrected p values are given. B) Genes identified as part of the glucose metabolic pathway in panel A depicted as relative values to illustrate the high association between dose and gene expression.
doi:10.1371/journal.pone.0048311.g004

maternal-placental-fetal tissues to deconjugate sulfated estrogens [32]. Total serum E2 during this period is in the range of 300 pM [33], and thus the low doses of E2 used in this study are physiologically relevant.

These microarray experiments were performed as a hypothesis generation step for a study of effects of estrogens on prostate development and differentiation, and the sample size is small. Because of this, the data must be seen as preliminary, but the results do indicate activation of different patterns of gene expression and dominance of different pathways at low, physiologically relevant, compared to high, pharmacological, doses of E2. Results from the lowest (10 pM and 100 pM) doses of E2

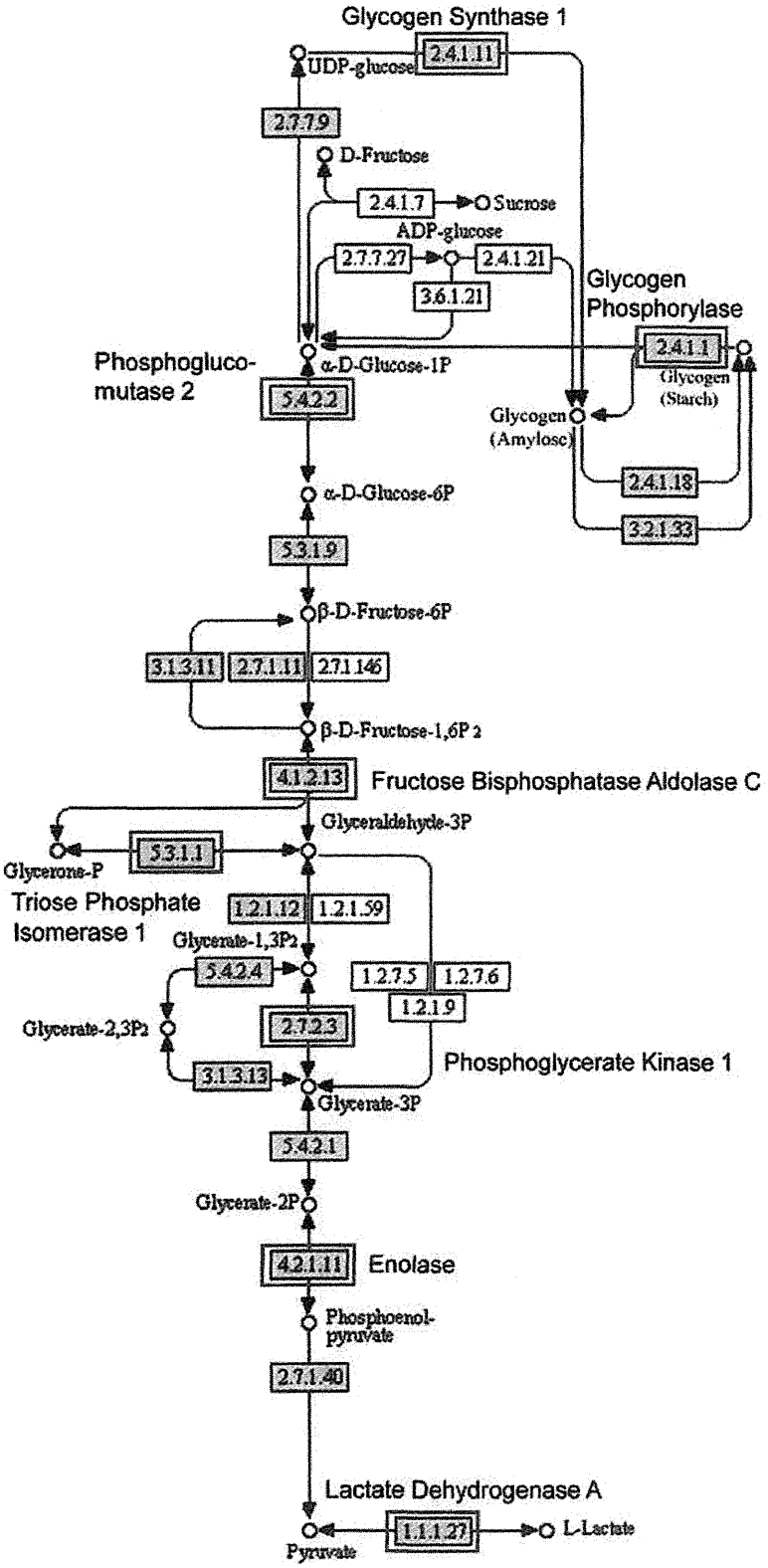

Figure 5. Glucose metabolism pathway. Highlighted genes (outlined in red) were influenced by lower dose estradiol treatment (10 pM and 100 pM) in an inverted U manner, suggesting enhancement of glycolysis by 10 pM E2 but suppression by 100 pM E2.
doi:10.1371/journal.pone.0048311.g005

Table 1. Functional characterization by gene ontology (GO) terms of gene expression profiles in cells treated with 100 nM E2.

		Number of genes		z-scores	
Category	**Gene Ontology Term**	**up-regulated**	**down- regulated**	**up-regulated**	**down- regulated**
Biological process	metabolic process	121	69	−2.08*	−1.43
	biological regulation	100	40	2.70**	−0.99
	growth	17	3	5.11**	−0.03
	reproduction	11	9	0.94.	2.02*
	reproductive process	5	6	0.42.	2.42*
	rhythmic process	6	1	3.92**	0.23
Molecular function	catalytic activity	135	76	−2.3*	0.82
	transporter activity	53	35	2.76**	1.42

doi:10.1371/journal.pone.0048311.t001

treatments indicate E2-inducible genes within pathways related to cell adhesion, actin cytoskeleton reorganization, EGF-like calcium binding, sterol biosynthesis and lipoprotein metabolism, and E2-suppressible genes within pathways related to growth factor signaling, tube development and additional effects on cell adhesion. At the high (100 nM) concentration, E2 induced genes enriched for steroid hormone signaling and metabolism, cytokines and their receptors, cell-to-cell communication, and TGF-β signaling (Table 2). Results from the 100 nM E2 treatment thus indicated effects on cell adhesion pathways, but also emphasized a stimulation of a positive feedback loop involving steroid hormone receptors and genes related to growth and metabolism that promote rather than inhibit cell growth. Taken together, these results suggest that fetal prostate mesenchymal cells may regulate epithelial cells through direct cell contacts when estrogen levels in mesenchyme are in the pM range, whereas growth factors might play significant roles when estrogen levels are higher in the nM range.

Importantly, an inverted U (non-monotonic) response was seen within the low-dose results, with enhancement of glycolysis observed at 10 pM E2 but significant suppression at 100 pM E2 (Figure 5). The expression of these specific genes was not influenced by 100 nM E2, indicating that the stimulation of glycolysis is highly dependent on dose and only seen at low pM E2 concentrations. This is of particular interest given the Warburg effect, the observation that most cancer cells rely on glycolysis to generate the energy needed for cellular processes, in contrast to normal differentiated cells that use mitochondrial oxidative phosphorylation [34–35]. The enhancement of glycolysis seen in our culture was only at the lowest dose tested here, 10 pM (2.72 pg/ml), and as such is intriguing because mice exposed prenatally to a very similar concentration of estradiol have enlarged prostates in adulthood [11] relative to mice exposed to higher doses. It is interesting to speculate on whether there is a relationship between the enhancement of cell proliferation rate and glycolysis seen in cancer cells, and the enhancement of glycolysis in fetal prostate mesenchymal cells and increased prostate size due to hyperplasia seen in mice.

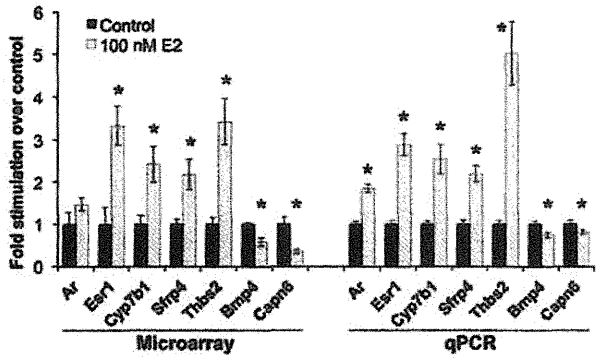

Figure 6. Comparison of expression of selected genes measured by microarray and by Q-PCR. Gene expression in cells treated with 100 nM 17β-estradiol (grey bars) is compared to that in untreated control cells (black bars). * Control vs. treated cells statistically different, $p<0.05$. The qPCR data were previously published elsewhere [19].

doi:10.1371/journal.pone.0048311.g006

Only 29 genes out of those screened were influenced by all doses of estradiol examined (Table 3). For approximately half of these genes the dose-response relationship was monotonic, although some of these were maximally up- or down-regulated at the 100 pM dose. For the rest, the direction of the effect (stimulation or suppression of gene expression) was either strongly reversed at the highest (100 nM) E2 concentration (a non-monotonic response), or simply showed a suggestion of reversal at the highest dose. Of the monotonic profiles, two genes showed particularly strong linearity with dose: Angpt2 (angiopoetin 2) and Sprr1a (small proline-rich protein 1a). Angpt2 expression is strongly correlated with prostate cancer progression [36] and is stimulated by growth factors, especially VEGF [37–38]; Vegf expression is stimulated by androgen treatment in fetal prostate fibroblasts [39], but we did not observe an effect of estrogen on Vegf expression here. Expression of Sprr genes is typically restricted to cells committed to terminal differentiation [40]. Although strong up-regulation of Sprr1a has been associated with abnormal cell differentiation in uterine tissue from neonatal CD-1 mice treated with diethylstilbestrol [41], effects in the developing prostate have not previously been reported.

Also of interest in this 29-gene subset are the clear inverse U effects on Perp and Gja1 expression. Perp is typically upregulated during apoptosis [42] but is also important for promoting desmosomal cell-cell adhesion [43], and loss of Perp is associated with dysregulation of cell adhesion and promotion of tumor development and progression [44]. Decreased expression of Gja1 (Cx43) is similarly consistent with loss or reduction of cell-cell communication. Only one gene in this 29-gene subset, Enpp2, showed a U-shaped response to increasing E2 concentrations; Enpp2 codes for autoaxin, an ecto-enzyme responsible for

Table 2. Effects of 100 nM estradiol treatment on gene expression within specific regulatory pathways identified as being of interest.

Pathway/Category	Direction	Ratio	Gene Identifier	Gene Name
Cell Communication	Up	2.50	AV239646	Gjb2
z-score (up) = 3.32	Up	1.96	BE197934	Krt1-14
	Up	2.62	AV330726	Gja1
	Up	*3.16*	*BC006894*	*Gja1*
	Up	*3.81*	*M63801*	*Gja1*
	Up	4.48	L06421	Thbs2
	Up	*3.43*	*NM_011581*	*Thbs2*
	Up	1.83	BI455189	Col6a2
Androgen and estrogen metabolism	Down	7.25	NM_023135	Sult1e1
z-score (up) = 2.4	Up	2.42	NM_007825	Cyp7b1
	Up	8.12	NM_01378	Hsd17b9
TGF-beta signaling pathway	Down	1.93	NM_010496	Idb2
z-score (down) = 2.19	Down	1.83	NM_008046	Fst
	Down	1.75	NM_007554	Bmp4
	Down	3.27	BM230984	Tgfb14i
	Up	3.67	BB353211	Inhbb
	Up	4.48	L06421	Thbs2
	Up	*3.43*	*NM_011581*	*Thbs2*
Steroid hormone receptors	Up	3.34	NM_007956	Esr1
	Up	5.29	NM_008829	Pgr
Wnt signaling	Down	2.22	NM_009519	Wnt11
	Up	3.72	NM_009526	Wnt6
	Up	1.89	W29605	Wnt7b
	Up	5.85	NM_020265	Dkk2
	Up	2.18	BB221995	Sfrp4
Cytokine-cytokine Receptor interaction	Up	2.77	NM_019583	Il17rb
	Up	2.21	NM_011330	Ccl11
	Up	6.53	NM_021443	Ccl8
	Up	3.67	BB353211	Inhbb
	Up	3.85	AF000304	Il4ra
	Up	*2.91*	*NM_010557*	*Il4ra*
Hedgehog signaling	Down	2.22	NM_009519	Wnt11
	Down	1.75	NM_007554	Bmp4
	Up	3.72	NM_009526	Wnt6
	Up	1.89	W29605	Wnt7b
Apoptosis	Up	2.07	BF137345	Birc4
	Down	2.85	NM_007603	Capn6
	Down	*2.23*	*AI747133*	*Capn6*
Prostate cancer	Up	3.40	BC010786	Creb3l3
	Up	2.21	AJ252157	Foxo1
	Up	2.60	NM_019739	Foxo1
Basal cell carcinoma	Down	2.22	NM_009519	Wnt11
	Down	1.75	NM_007554	Bmp4
	Up	3.72	NM_009526	Wnt6
	Up	1.89	W29605	Wnt7b

All genes listed are significantly altered at $P<0.05$. Where the z-score for the entire pathway was significant, the score is given below the pathway name. Where multiple probes for the same gene are represented in these lists (indicated by italics), agreement was good between the probes.

doi:10.1371/journal.pone.0048311.t002

Table 3. Genes whose expression was significantly (P≤0.05) influenced by estradiol (E2) treatment at all doses tested.

		Log2 fold expression relative to control				
Low-dose cluster group	**Gene ID**	**No E2**	**10 pM E2**	**100 pM E2**	**100 nM E2**	**Monotonic trend?**
Inducible_moderate	Sprr1a	0.00	0.98	2.23	5.57	Y
Inducible_moderate	Angpt2	0.00	1.20	2.25	3.77	Y
Inducible_moderate	Dkk2	0.00	0.67	2.21	2.55	Y
Inducible_moderate	Pgr	0.00	0.98	2.22	2.40	Y
Inducible_low	Fabp7	0.00	0.75	2.18	2.26	Y
Inducible_low	Fbxo32	0.00	−0.33	1.52	1.57	Y
Inducible_moderate	Esr1	0.00	1.00	2.19	1.74	I
Inducible_moderate	Rgs4	0.00	0.64	2.09	1.81	I
Inducible_moderate	Thbs2	0.00	1.49	2.20	1.78	I
Inducible_moderate	Btbd3	0.00	0.95	2.25	1.05	N
Inducible_moderate	Gja1	0.00	0.66	2.21	1.51*	N
Inducible_moderate	Npy1r	0.00	1.14	2.16	1.49	N
Inducible_low	Perp	0.00	0.21	2.06	0.71	N
Suppressible_low	Sult1e1	0.00	0.20	−1.81	−2.86	Y
Suppressible_low	Lcn2	0.00	0.49	−1.63	−2.44	Y
Suppressible_low	Egfl6	0.00	−0.20	−2.04	−1.93	Y
Suppressible_low	Pdlim3	0.00	−0.14	−1.96	−1.95	Y
Suppressible_low	Cdkn1c	0.00	−0.19	−1.99	−1.16	Y
Suppressible_low	Capn6	0.00	−0.43	−1.93	−1.51	I
Suppressible_low	Igfbp2	0.00	0.15	−1.87	−0.96	I
Suppressible_low	Wnt11	0.00	−0.55	−2.11	−1.15	I
Suppressible_low	Cyb561	0.00	0.57	−1.52	−0.93	I
Suppressible_low	Gda	0.00	−0.49	−2.06	−0.77	I
Suppressible_low	Dpep1	0.00	0.97	−1.19	−0.67	I
Suppressible_low	Zfp161	0.00	0.10	−1.70	0.74	N
Suppressible_low	Sfrp4	0.00	0.16	−1.77	1.12	N
Suppressible_low	Penk1	0.00	−0.53	−1.95	1.06	N
Suppressible_low	Enpp2	0.00	0.90	−1.17	1.85	N
U-curve	Cd80	0.00	−1.04	1.12	0.65	I

For each gene the log2 value of the fold change is given, and thus up-regulated and down-regulated genes are reflected in positive and negative numbers respectively. Genes are sorted first according to the cluster groups identified for the low-dose treatments (see Methods), and then by whether the trend at the high dose (100 nM) is consistent with the results seen at lower doses. Y = monotonic trend; gene expression at 100 nM E2 continues the trend at lower doses or has reached a plateau at that point. N = trend is clearly not monotonic; gene expression at 100 nM E2 is in the reverse direction of the trend at lower doses. I = suggestion of non-monotonic trend; gene expression at 100 nM shows slight reversal of trend at lower doses. *Value is average value for all probes for this gene (n = 5).

doi:10.1371/journal.pone.0048311.t003

producing lysophophatidic acid (LPA), known to be a mitogen for both ovarian and prostate cancer cells, which stimulates cell proliferation, survival and migration (reviewed in [45]). These non-monotonically expressed genes reinforce the general conclusion that pathways related to cell adhesion are influenced by estrogen treatment, but also suggest a different effect of the highest dose relative to the lower doses, with a progression toward increased cell proliferation and migration at increasing dose.

The Wnt signaling pathway was influenced at all E2 doses examined, but with an emphasis toward up-regulation of canonical Wnt/β-catenin stabilization signaling at the high dose, and non-canonical (PCP) signaling at lower doses. The high-dose effect may be mediated through the known association of β-catenin with AR and ER. Truica *et al.* have shown that β-catenin significantly enhances androgen-stimulated transcriptional activation by the AR, and that β-catenin also increases AR transcriptional activation by E2 [46]. Although many Wnt genes are differentially expressed in the prostate according to age [47], their role in prostate development, and particularly their interactive and temporal roles, is only starting to be described.

At the high dose of E2 we observed changes in genes related to steroid hormone metabolism, and alterations in steroid hormone signaling that would lead in turn to disruption of the normal expression of other developmentally important genes. Of particular interest was the observed up-regulation of Cyp7b1, which catalyzes the metabolism of the DHT metabolites 3α-Adiol and 3β-Adiol, and is thought to control cellular levels of both androgens and estrogens [48]. We verified by quantitative PCR (qPCR) that the up-regulation of Esr1 observed in these estrogen-treated cells was dose-dependent and consistent with our prior data ([14], data not shown); up-regulation of Ar was seen by qPCR but did not reach statistical significance by microarray. Esr1 was stimulated across the entire E2 dose range in this study, and thus is a potential common mechanism for the initiation of consequent

signaling events. Stimulation of Esr1 and Ar serve to amplify estrogen and androgen signaling respectively, and in the intact gland there would be further potential for signal amplification, with local conversion of testosterone not only via Srd5a1 to the more potent androgen DHT, but also via aromatization to E2.

It is important to note that the intracellular concentration of E2 within the urogenital sinus during development is still unknown. The dose of E2 that reaches ER in male mouse UGS mesenchyme cells would depend not only on E2 uptake from the blood but also on local aromatization of testosterone to E2. Because of this issue, we administered E2 over a wide dose range, but also ensured that the opportunity for aromatization was controlled by the use of DHT rather than testosterone in the culture medium. Total testosterone circulates in the range of 5–8 nM in the male rat and mouse fetus during prostate differentiation [11,32]. Because there is no high-affinity testosterone binding protein in the blood at this time, and testosterone is only weakly bound to albumin, the result is that the percentage of total testosterone in blood that is bioactive is high, particularly compared to E2, which binds to the high-affinity plasma protein alphafetoprotein. Serum testosterone thus provides a substantial pool from which intracellular E2 can be formed by aromatization in fetal prostate mesenchyme cells [32,49]. Arase and colleagues [50] have measured E2 concentrations in fetal male mouse UGS tissue at GD17 and postnatal day (PD) 1, which approximated 10 and 25 pg/g, respectively. These concentrations are consistent with the low doses of E2 that we administered in this study, although again we do not know how much of this E2 reaches ER (the actual dose at target). Future work should address the dynamics of estrogen concentration and receptor activation both *in vitro* and *in vivo*.

The up-regulation of Pgr by all doses of E2 administered here to UGS mesenchyme cells is in general agreement with Risbridger et al., who reported up-regulation of progesterone receptors (PR) in the adult mouse prostate after estrogen treatment [51], and with data from Nishino et al. that showed enhancement of progesterone's proliferative effects on the adult rat prostate after co-treatment with E2 or DHT [52]. The presence of PR may be more relevant during fetal life, when progesterone levels are higher, than in adulthood when progesterone levels are low. The issue of fetal responsiveness to progestins is complex in that there is evidence that progestins can have anti-androgenic influences on sexual differentiation, through inhibition of 5α-reductase [53,54]. Up-regulation of Pgr is thus a potential mechanism for disruptive effects of estrogens on male accessory reproductive organ development, but its impact will require further study.

Neonatal estrogen treatment is known to affect the expression of several genes critical to prostate development. Notable examples are Hoxb13, Nkx3.1, Shh, Fgf10 and Bmp4 [55]. Some of the genes that responded to E2 treatment in our cells agree with the findings of others (Hoxb13, Bmp4), but several of the "candidate" genes were not affected at the doses we examined. There may be several reasons for this, but two are critical. First, we deliberately cultured only the mesenchyme cells, to specifically examine effects of E2 on gene expression in the cells that initiate early prostate differentiation. Without the two-way communication that occurs between epithelial and mesenchymal cells in the developing prostate the full range of gene expression will not be seen [1,56,57]. For example, Nkx3.1 is expressed only in epithelial cells in regions of ductal growth, although its expression is dependent on the presence of UGS mesenchyme [58]. Similarly, Ptc and Gli, components of the Shh signaling pathway that are important for directing ductal growth, are expressed in the mesenchyme but are regulated by Shh signaling from the epithelium [59]. Additionally, in studies performed *in vivo*, other factors provided via blood circulation (known or unknown), as well as shifts in hormone levels that occur during late fetal life, parturition and early postnatal life [32,59], will influence gene expression. Consequently, studies performed in whole tissues of intact animals are bound to yield different and more complex results.

Developmental estrogen exposure has the potential to acutely stimulate abnormal growth and induction of hyperplasia in the developing prostate [12], and this clearly establishes the potential for abnormal function in later life and a predisposition toward adult prostate disease [28]. The growth of fetal prostate epithelial cells and duct formation are driven by signals from the UGS mesenchyme [9], and our results suggest that the developmental effects of estrogens or xenoestrogens on UGS differentiation may be mediated initially by enhanced mesenchymal cell responsiveness to sex steroid hormones through up-regulation of steroid hormone receptor concentrations, with subsequent effects on other genes that differed based on the dose of E2. The differing patterns of gene expression at low and high E2 concentrations and the presence of non-monotonic responses of some genes to the wide (10,000-fold) range of E2 concentrations studied are consistent with non-monotonic dose effects on prostate development *in vivo* [11,12,13].

Supporting Information

Article S1 Previously published article [19] that included qPCR data from validation tests for microarray experiments. The data presented (Figure 5, page 89) show effects of 100 nM estradiol on expression of seven genes, and effects of 1000 nM bisphenol A on the same seven genes. Microarray data are not included.
(PDF)

Author Contributions

Conceived and designed the experiments: FVS CAR. Performed the experiments: JAT CAR AS KC HW. Analyzed the data: JAT KC TS CAR. Contributed reagents/materials/analysis tools: FVS TS TI . Wrote the paper: JAT FVS TS.

References

1. Marker PC, Donjacour AA, Dahiya R, Cunha GR (2003) Hormonal, cellular, and molecular control of prostatic development. Developmental Biology 253: 165–174.
2. Prins GS, Putz O (2008) Molecular signaling pathways that regulate prostate gland development. Differentiation 76: 641–659.
3. Richter CA, Timms BG, vom Saal FS (2005) Prostate Development: Mechanisms for opposite effects of low and high doses of estrogenic chemicals. In: Naz RK, editor. Endocrine Disruptors (2nd Edition): Effects on Male and Female Reproductive Systems. Boca Raton, FL: CRC Press. pp. 379–410.
4. Cunha GR, Donjacour A (1987) Stromal-epithelial interactions in normal and abnormal prostatic development. Progress in Clinical & Biological Research 239: 251–272.
5. Kokontis JM, Liao S (1999) Molecular action of androgen in the normal and neoplastic prostate. Vitamins and Hormones 55: 219–307.
6. Cooke PS, Young P, Cunha GR (1991) Androgen receptor expression in developing male reproductive organs. Endocrinology 128: 2867–2873.
7. Prins GS, Birch L (1997) Neonatal estrogen exposure up-regulates estrogen receptor expression in the developing and adult rat prostate lobes. Endocrinology 138.
8. Timms BG, Petersen SL, vom Saal FS (1999) Prostate gland growth during development is stimulated in both male and female rat fetuses by intrauterine proximity to female fetuses. Journal of Urology 161: 1694–1701.
9. Cunha GR, Ricke W, Thomson A, Marker PC, Risbridger G, et al. (2004) Hormonal, cellular, and molecular regulation of normal and neoplastic prostatic development. Journal of Steroid Biochemistry and Molecular Biology 92: 221–236.

10. Omoto Y, Imamov O, Warner M, Gustafsson J-Å (2005) Estrogen receptor a and imprinting of the neonatal mouse ventral prostate by estrogen. Proceedings of the National Academy of Sciences 102: 1484–1489.
11. vom Saal FS, Timms BG, Montano MM, Palanza P, Thayer KA, et al. (1997) Prostate enlargement in mice due to fetal exposure to low doses of estradiol or diethylstilbestrol and opposite effects at high doses. Proceedings of the National Academy of Sciences of the United States of America 94: 2056–2061.
12. Timms BG, Howdeshell KL, Barton L, Bradley S, Richter CA, et al. (2005) Estrogenic chemicals in plastic and oral contraceptives disrupt development of the mouse prostate and urethra. Proceedings of the National Academy of Sciences U S A 102: 7014–7019.
13. Gupta C (2000) Reproductive malformation of the male offspring following maternal exposure to estrogenic chemicals. Proc Soc Exp Biol Med 224: 61–68.
14. Richter CA, Taylor JA, Ruhlen RL, Welshons WV, vom Saal FS (2007) Estradiol and Bisphenol A Stimulate Androgen Receptor and Estrogen Receptor Gene Expression in Fetal Mouse Prostate Mesenchyme Cells. Environmental Health Perspectives 115: 902–908.
15. Prins GS, Birch L, Greene GL (1991) Androgen receptor localization in different cell types of the adult rat prostate. Endocrinology 129: 3187–3199.
16. Ellem SJ, Risbridger GP (2006) Aromatase and prostate cancer. Minerva Endocrinol 31: 1–12.
17. Nonneman DJ, Ganjam VK, Welshons WV, Vom Saal FS (1992) Intrauterine position effects on steroid metabolism and steroid receptors of reproductive organs in male mice. Biol Reprod 47: 723–729.
18. Nolan T, Hands RE, Bustin SA (2006) Quantification of mRNA using real-time RT-PCR. Nature Protocols 1: 1559–1582.
19. Taylor JA, Richter CA, Ruhlen RL, vom Saal FS (2011) Estrogenic environmental chemicals and drugs: Mechanisms for effects on the developing male urogenital system. Journal of Steroid Biochemistry and Molecular Biology 127: 83–95.
20. Bustin SA (2000) Absolute quantification of mRNA using real-time reverse transcription polymerase chain reaction assays. Journal of Molecular Endocrinology 25: 169–193.
21. Latil A, Bieche I, Vidaud D, Lidereau R, Berthon P, et al. (2001) Evaluation of androgen, estrogen (ER alpha and ER beta), and progesterone receptor expression in human prostate cancer by real-time quantitative reverse transcription-polymerase chain reaction assays. Cancer Research 61: 1919–1926.
22. Reimand MK, Arak T, Vilo J (2011) g:Profiler – a web server for functional interpretation of gene lists (2011 update) Nucleic Acids Research 39: W307–W315.
23. Reimand MK, Peterson H, Hansen J, Vilo J (2007) g:Profiler – a web-based toolset for functional profiling of gene lists from large-scale experiments. Nucleic Acids Research 35: W193–W200.
24. Huang DW, Sherman BT, Lempicki RA (2009) Systematic and integrative analysis of large gene lists using DAVID bioinformatics resources. Nature Protocols 4: 44–57.
25. Huang DW, Sherman BT, Lempicki RA (2009) Bioinformatics enrichment tools: paths toward the comprehensive functional analysis of large gene lists. Nucleic Acids Research 37: 1–13.
26. Thayer KA, Ruhlen RL, Howdeshell KL, Buchanan DL, Cooke PS, et al. (2001) Altered prostate growth and daily sperm production in male mice exposed prenatally to subclinical doses of 17alpha-ethinyl oestradiol. Human Reproduction 16: 988–996.
27. Prins GS, Birch L, Tang WY, Ho SM (2007) Developmental estrogen exposures predispose to prostate carcinogenesis with aging. Reprod Toxicol 23: 374–382.
28. Ho SM, Tang WY, Belmonte de Frausto J, Prins GS (2006) Developmental exposure to estradiol and bisphenol A increases susceptibility to prostate carcinogenesis and epigenetically regulates phosphodiesterase type 4 variant 4. Cancer Research 66: 5624–5632.
29. Jirasek J (1980) Normal development of the male accessory glands. In: Spring-Mills EaH, E.S.E., editor. Male Accessory Sex Glands. New York Elsevier North-Holland Biomedical Press. pp. 3–37.
30. Rajfer J, Coffey DS (1979) Effects of neonatal steroids on male sex tissues. Investigative Urology 17: 3–8.
31. Coser KR, Chesnes J, Hur J, Ray S, Isselbacher KJ, et al. (2003) Global analysis of ligand sensitivity of estrogen inducible and suppressible genes in MCF7/BUS breast cancer cells by DNA microarray. Proc Natl Acad Sci U S A 100: 13994–13999.
32. vom Saal FS, Montano MM, Wang MH (1992) Sexual differentiation in mammals. In: Colborn T, Clement C, editors. Chemically induced alterations in sexual and functional development: the wildlife/human connection. Princeton: Princeton Scientific Publishing Co. pp. 17–83.
33. Nagel SC, vom Saal FS (2003) Endocrine control of sexual differentiation: Effects of the maternal-fetal environment and endocrine disrupting chemicals. In: Miller V, Hay M, editors. Principles of Sex-Based Physiology. New York: Elsevier. pp. 15–37.
34. Warburg O (1956) On the origin of cancer cells. Science 123: 309–314.
35. Kim JW, Dang CV (2006) Cancer's molecular sweet tooth and the Warburg effect. Cancer Res 66: 8927–8930.
36. Lind AJ, Wikstrom P, Granfors T, Egevad L, Stattin P, et al. (2005) Angiopoietin 2 expression is related to histological grade, vascular density, metastases, and outcome in prostate cancer. Prostate 62: 394–399.
37. Shih SC, Robinson GS, Perruzzi CA, Calvo A, Desai K, et al. (2002) Molecular profiling of angiogenesis markers. Am J Pathol 161: 35–41.
38. Winter SF, Acevedo VD, Gangula RD, Freeman KW, Spencer DM, et al. (2007) Conditional activation of FGFR1 in the prostate epithelium induces angiogenesis with concomitant differential regulation of Ang-1 and Ang-2. Oncogene 26: 4897–4907.
39. Levine AC, Liu XH, Greenberg PD, Eliashvili M, Schiff JD, et al. (1998) Androgens induce the expression of vascular endothelial growth factor in human fetal prostatic fibroblasts. Endocrinology 139: 4672–4678.
40. Hohl D, de Viragh PA, Amiguet-Barras F, Gibbs S, Backendorf C, et al. (1995) The small proline-rich proteins constitute a multigene family of differentially regulated cornified cell envelope precursor proteins. J Invest Dermatol 104: 902–909.
41. Huang WW, Yin Y, Bi Q, Chiang TC, Garner N, et al. (2005) Developmental diethylstilbestrol exposure alters genetic pathways of uterine cytodifferentiation. Mol Endocrinol 19: 669–682.
42. Attardi LD, Reczek EE, Cosmas C, Demicco EG, McCurrach ME, et al. (2000) PERP, an apoptosis-associated target of p53, is a novel member of the PMP-22/gas3 family. Genes Dev 14: 704–718.
43. Ihrie RA, Marques MR, Nguyen BT, Horner JS, Papazoglu C, et al. (2005) Perp is a p63-regulated gene essential for epithelial integrity. Cell 120: 843–856.
44. Beaudry VG, Jiang D, Dusek RL, Park EJ, Knezevich S, et alLoss of the p53/p63 regulated desmosomal protein Perp promotes tumorigenesis. PLoS Genet 6: e1001168.
45. Mills GB, Moolenaar WH (2003) The emerging role of lysophosphatidic acid in cancer. Nat Rev Cancer 3: 582–591.
46. Truica CI, Byers S, Gelmann EP (2000) Beta-catenin affects androgen receptor transcriptional activity and ligand specificity. Cancer Research 60: 4709–4713.
47. Zhang TJ, Hoffman BG, Ruiz de Algara T, Helgason CD (2006) SAGE reveals expression of Wnt signalling pathway members during mouse prostate development. Gene Expression Patterns 6: 310–324.
48. Pettersson H, Lundqvist J, Oliw E, Norlin M (2009) CYP7B1-mediated metabolism of 5alpha-androstane-3alpha,17beta-diol (3alpha-Adiol): a novel pathway for potential regulation of the cellular levels of androgens and neurosteroids. Biochim Biophys Acta 1791: 1206–1215.
49. Danzo BJ, Eller BC (1985) The ontogeny of biologically active androgen-binding protein in rat plasma, testis, and epididymis. Endocrinology 117: 1380–1388.
50. Arase S, Ishii K, Igarashi K, Aisaki K, Yoshio Y, et al. (2011) Endocrine disrupter bisphenol a increases in situ estrogen production in the mouse urogenital sinus. Biol Reprod 84: 734–742.
51. Risbridger GP, Wang H, Frydenberg M, Cunha G (2001) The metaplastic effects of estrogen on mouse prostate epithelium: proliferation of cells with basal cell phenotype. Endocrinology 142: 2443–2450.
52. Nishino T, Ishibashi K, Hirtreiter C, Nishino Y (2009) The prostate growth stimulation by progesterone is due to androgenic products and progesterone receptor-mediated mechanisms. Pharmazie 64: 587–589.
53. Dean HJ, Winter JS (1984) The effect of five synthetic progestational compounds on 5 alpha-reductase activity in genital skin fibroblast monolayers. Steroids 43: 13–24.
54. Wagner CK, Kinsley C, Svare B (1986) Mice: postpartum aggression is elevated following prenatal progesterone exposure. Hormones and Behavior 20: 212–221.
55. Huang L, Pu Y, Alam S, Birch L, Prins G (2004) Estrogenic Regulation of Signaling Pathways and Homeobox Genes During Rat Prostate Development. Jounal of Andrology 25: 330–337.
56. Cunha GR, Fujii H, Neubauer BL, Shannon JM, Sawyer L, et al. (1983) Epithelial-mesenchymal interactions in prostatic development. I. morphological observations of prostatic induction by urogenital sinus mesenchyme in epithelium of the adult rodent urinary bladder. Journal of Cell Biology 96: 1662–1670.
57. Timms BG, Lee CW, Aumuller G, Seitz J (1995) Instructive induction of prostate growth and differentiation by a defined urogenital sinus mesenchyme. Microscopy Research and Technique 30: 319–332.
58. Shen MM, Abate-Shen C (2003) Roles of the Nkx3.1 homeobox gene in prostate organogenesis and carcinogenesis. Developmental Dynamics 228: 767–778.
59. Lamm ML, Catbagan WS, Laciak RJ, Barnett DH, Hebner CM, et al. (2002) Sonic hedgehog activates mesenchymal Gli1 expression during prostate ductal bud formation. Developmental Biology 249: 349–366.

Induction of Rapid T Cell Death and Phagocytic Activity by Fas-Deficient *lpr* Macrophages

Ritsuko Oura,*,† Rieko Arakaki,* Akiko Yamada,* Yasusei Kudo,* Eiji Tanaka,† Yoshio Hayashi,* and Naozumi Ishimaru*

Peripheral T cells are maintained by the apoptosis of activated T cells through the Fas–Fas ligand system. Although it is well known that normal T cells fail to survive in the Fas-deficient immune condition, the molecular mechanism for the phenomenon has yet to be elucidated. In this study, we demonstrate that rapid cell death and clearance of normal T cells were induced by Fas-deficient *lpr* macrophages. Transfer of normal T cells into *lpr* mice revealed that Fas expression on donor T cells was promptly enhanced through the IFN-γ/IFN-γR. In addition, Fas ligand expression and phagocytic activity of *lpr* macrophages were promoted through increased NF-κB activation. Controlling Fas expression on macrophages plays an essential role in maintaining T cell homeostasis in the peripheral immune system. Our data suggest a critical implication to the therapeutic strategies such as transplantation and immunotherapy for immune disorder or autoimmunity related to abnormal Fas expression. *The Journal of Immunology*, 2013, 190: 578–585.

The Fas receptor is expressed on most tissues and plays an important role in regulating the normal function of many different organs. Fas signaling can regulate T cell and B cell differentiation, maturation, activation, and deletion in the peripheral immune system (1–3). Activation-induced cell death (AICD) is involved in the removal of activated T cells in vivo and depends on Fas and Fas ligand (FasL) (4, 5). Among apoptotic mechanisms, AICD plays a central role in the removal of autoreactive T cells and in prevention of autoimmune responses (6).

MRL/Mp mice bearing a Fas deletion mutant gene, *lpr* (MRL/*lpr*), spontaneously develop autoimmune lesions resembling human glomerulonephritis, arthritis, vasculitis, and Sjögren's syndrome (7–10). In addition, *gld* mice defective in the FasL gene exhibit autoimmune lesions (11). Both strains lack the cell death mechanism mediated through the Fas–FasL interaction in the immune system. Ligation of Fas by the homotrimeric FasL results in the clustering of Fas and recruitment of the adaptor protein Fas-associated death domain to clustered Fas intracellular death domains (5, 12–14). In addition, Fas and only the Bcl2 homology domain 3 (BH3-only protein) such as Bim play overlapping roles in peripheral T cell death in immune response shutdown and prevention of immune disorders (15). In contrast, the regulation of T cell susceptibility to AICD is controlled by T cell maturity and activation and the presence or absence of APCs such as macrophages or dendritic cells (5, 16).

Normal hematopoietic cells including spleen and bone marrow cells do not survive in *lpr* mice (17, 18). In addition, it was reported that in vitro coculture of normal and *lpr*-derived T cell lines resulted in the loss of the normal T cells (17, 19). These in vivo and in vitro findings could be explained by the elevated FasL expression on *lpr* immune cells (20, 21). However, the precise mechanism underlying the FasL overexpression in *lpr* immune cells or the association of normal T cell deletion with APCs in Fas-deficient *lpr* mice remains unclear.

In this study, we focused on T cell apoptosis in Fas-deficient recipients using C57BL/6/*lpr* mice to define the cellular and molecular mechanisms of AICD in T cells and the regulation of FasL expression. Furthermore, we investigated whether macrophages in Fas-deficient *lpr* mice contribute to the clearance of apoptotic T cells in the peripheral immune system.

Materials and Methods

Mice

C57BL/6 (B6), B6-*lpr*/*lpr* (B6/*lpr*), and B6-*gld*/*gld* (B6/*gld*) mice were purchased from Japan SLC Laboratory (Shizuoka, Japan). OT-II mice (C57BL/6-Tg (TcraTcrb) 425Cbn/J) and IFN-γR gene knockout (*IFNγR*$^{-/-}$) mice were obtained from Dr. J. Sprent. *NF-κB*$_1$$^{-/-}$ mice were obtained from The Jackson Laboratory. GFP-transgenic (TG) mice were obtained from RIKEN BioResource Center (Tsukuba, Japan). All mice were bred at the animal facility of the University of Tokushima under specific pathogen-free conditions. The experiments were approved by an animal ethics board of the University of Tokushima.

Adoptive cell transfer

T cells were purified from the spleen of B6, GFP-TG, OT-II, B6/*lpr*, or *IFNγR*$^{-/-}$ mice using Abs including anti-MHC class II, anti-B220 (eBioscience, San Diego, CA), and immunomagnetic beads (Dynal, Oslo, Norway). T cells from all mice, except GFP-TG mice, were labeled with CFSE (Invitrogen, Carlsbad, CA). A total of 1, 2, or 5 × 10^6 T cells were i.v. or i.p. transferred into B6, B6/*lpr*, B6/*gld*, or *NF-κB*$_1$$^{-/-}$/*lpr* mice. For homeostatic expansion, the recipient mice were irradiated at 8.5

*Department of Oral Molecular Pathology, Institute of Health Biosciences, University of Tokushima Graduate School, Tokushima 770-8504, Japan; and †Department of Orthodontics and Dentofacial Orthopedics, Institute of Health Biosciences, University of Tokushima Graduate School, Tokushima 770-8504, Japan

Received for publication December 28, 2011. Accepted for publication November 12, 2012.

This work was supported by the Funding Program for Next Generation World-Leading Researchers in Japan (Grant LS090) and by Grants-in-Aid for Scientific Research (17109016 and 17689049) from the Ministry of Education, Science, Sport and Culture of Japan.

Address correspondence and reprint requests to Dr. Naozumi Ishimaru, Department of Oral Molecular Pathology, Institute of Health Biosciences, University of Tokushima Graduate School, 3-18-15 Kuramotocho, Tokushima 770-8504, Japan. E-mail address: ishimaru@dent.tokushima-u.ac.jp

The online version of this article contains supplemental material.

Abbreviations used in this article: AICD, activation-induced cell death; B6, C57BL/6; B6/*gld*, C57BL/6-*gld*/*gld*; B6/*lpr*, C57BL/6-*lpr*/*lpr*; FasL, Fas ligand; *IFNγR*$^{-/-}$, IFN-γR gene knockout; LN, lymph node; PEC, peritoneal exudate cell; TG, transgenic.

www.jimmunol.org/cgi/doi/10.4049/jimmunol.1103794

Gy before T cell transfer. For the analysis of donor T cells, spleen cells, lymph node (LN) cells, PBMCs, or peritoneal exudate cells (PECs) were analyzed by flow cytometry. To inhibit in vivo deletion of T cells, anti-FasL mAb (clone MFL3; BioLegend, San Diego, CA) was i.p. injected into recipient mice together with transfer of T cells.

Flow cytometry

FITC, PE, allophycocyanin–peridin chlorophyll protein, PE-Cy5.5, PE-Cy7, or allophycocyanin–Cy7-conjugated Abs including anti-CD4, CD8, CD11b, Fas, and FasL Abs, were used. A FACScan flow cytometer (BD Biosciences, Franklin Lakes, NJ) was used, and data were analyzed using the FlowJo FACS Analysis software (Tree Star, Ashland, OR).

In vivo imaging

The mice were s.c. injected with isoflurane (Abbott Laboratories, Abbot Park, IL) as an anesthetic. Purified T cells were incubated with XenoLight DiR (Caliper Life Sciences, Hopkinton, MA) for 30 min. A total of 5×10^6 T cells were i.v. transferred into recipient mice, and donor T cells were monitored at 30 min, 2 h, and 6 h using in vivo imaging analyzer (Caliper Life Sciences).

ELISA

The concentration of IFN-γ in sera was measured by ELISA. Ninety-six-well flat-bottom plates were precoated with capture Abs, and diluted samples or standard recombinant cytokines were added to each well. After the plates were washed, biotinylated Abs were added, and the wells were incubated with HRP-labeled, affinity-purified anti-rat IgG. A solution of *o*-phenylenediamine (Sigma-Aldrich, St. Louis, MO) was added to each well as the substrate. The optimal density at 490 nm was measured using a microplate reader (Model 680; Bio-Rad Laboratories, Richmond, CA).

Quantitative RT-PCR

Total RNA was extracted from spleen cells or PECs using Isogen (Wako Pure Chemical Industries, Osaka, Japan); it was then reverse transcribed. The transcript levels of FasL, TNF-α, IL-6, IL-1β, and β-actin were performed using a PTC-200 DNA Engine Cycler (Bio-Rad Laboratories) with SYBR Premix Ex Taq (Takara Bio, Shiga, Japan). The primer sequences used were as follows: FasL, forward, 5′-GTGGGCCGCTCTAGGCACCA-3′, and reverse, 5′-CGGTTGGCCTTAGGGTTCAGGGGG-3′; TNF-α, forward, 5′-ATGAGCACAGAAAGCATGATC-3′, and reverse, 5′-AGATGATCTGAGTGTGAGGG-3′; IL-6, forward, 5′-CTCTGCAAGAGAGACTTCCAT-3′, and reverse, 5′-ATAGGCAAATTTCCTGATTATA-3′; IL-1β, forward, 5′-TGATGAGAATGACCTGTTCT-3′, and reverse, 5′-CTTCTTCAAAGATGAAGGAAA-3′; β-actin, forward, 5′-GTGGGCCGCTCTAGGCACCA-3′, and reverse, 5′-CGGTTGGCCTTAGGGTTCAGGGGG-3′.

Preparation of peritoneal macrophages

Mice were i.p. injected with 1 ml 3% thioglycollate broth (Sigma-Aldrich), and after 3 or 4 d, elicited macrophages were collected by peritoneal lavage with 5 ml ice-cold PBS.

Phagocytosis assay

Phagocytosis was assessed using Fluoresbrite Yellow Green Caboxylate Microspheres (Polysciences, Warrington, PA). Briefly, the $CD11b^+$ cells purified from PECs were incubated with opsonized beads for 30 min at 37°C and washed with PBS. The phagocytic activity of $CD11b^+$ cells was evaluated by flow cytometric analysis.

Apoptosis detection assay

Apoptosis was detected using the Annexin V-FITC apoptosis detection kit (Bio Vision, Mountain View, CA). Briefly, the cells were washed with PBS and incubated with FITC-conjugated annexin V and propidium iodide for 15 min at room temperature in the dark. Binding buffer was added, and apoptotic cells were detected by flow cytometoric analysis. To inhibit in vitro T cell apoptosis cocultured with PECs, PECs were treated with a Fas-Fc fusion protein (R&D Systems, Minneapolis, MN).

Confocal microscopic analysis

PECs including GFP^+ T cells were stained with PE-conjugated anti-CD11b mAb (eBioscience) on a glass slide. Coverslips were applied with Fluoromount-G (Molecular Probe). Cells were visualized using a Confocal Laser Microscan (LSM 5 Pascal; Carl Zeiss, Oberkochen, Germany).

Western blot analysis

Cell extracts from the nucleus and cytoplasm of $CD11b^+$ PECs were prepared using NE-PER Nuclear and Cytoplasmic Extraction Reagents (Thermo Fisher Scientific, Rockford, IL). A total of 10 μg of each sample per well was used for SDS-PAGE. After blocking with 5% nonfat milk, the membrane was incubated with primary Abs against phospho-IκBα and p50 (NF-κB1), RelA (p65), and histones (Santa Cruz Biotechnology, Santa Cruz, CA). Ag–Ab complexes were detected using HRP-conjugated secondary Abs. Protein binding was visualized using the Phototope-HRP Western blot Detection System (Cell Signaling Technology, Danvers, MA).

NF-κB transcription activity assay

The transcription activity of NF-κB in the nuclear extracts from PECs was analyzed with a NF-κB transcription factor colorimetric assay kit (Millipore, Billerica, MA). Briefly, nuclear extracts were incubated with a biotinylated double-stranded oligonucleotide probe containing the consensus sequence for NF-κB on a streptavidin-coated plate. Captured complexes, including active NF-κB protein, were incubated with the primary Abs for p50 and RelA, HRP-conjugated secondary Ab, and tetramethylbenzidine substrate. The absorbance of the samples was measured using a microplate reader at 450 nm.

Statistical analysis

Statistical significance was determined with an unpaired the Student *t* test.

Results

Normal T cell dynamics in Fas-deficient mice

To understand the dynamics of normal T cells in Fas-deficient mice, the T cells from GFP-TG mice were i.v. transferred into B6 and B6/*lpr* mice. On 7 d after the transfer, GFP^+ cells in the spleen and LNs of the recipient mice were analyzed. Although GFP^+ T cells were found in the spleen and LNs of B6 mice, these cells were barely detectable in B6/*lpr* mice (Fig. 1A). To evaluate the in vivo expansion of normal T cells in Fas-deficient mice using a homeostatic proliferation system, CFSE-labeled normal T cells from B6 mice were i.v. transferred into irradiated B6 and B6/*lpr* mice. On 7 d after the transfer, expanded T cells were found in B6 mice (Fig. 1B). However, the transferred $CFSE^+$ T cells in the spleen and LNs of B6/*lpr* mice were almost undetectable (Fig. 1B). In addition, to examine the in vivo Ag-specific T cell response in B6/*lpr* mice, $CD4^+$ T cells were purified from the spleen of OVA-specific TCR-TG (OT-II) mice and were transferred into B6 and B6/*lpr* mice. OVA peptide (100 μg/mouse) was injected into the recipient mice on the following day. On 7 d after the transfer, OT-II–specific $V\beta5.2^+CD4^+$ T cells of the spleen and LNs were analyzed. Although OT-II T cells were found in the spleen and LNs of B6 recipients, these cells were almost undetectable in the spleen and LNs of B6/*lpr* mice (Fig. 1C). These findings indicate that normal T cells fail to migrate to lymphoid tissues or survive under the Fas-deficient environment. In addition, we examined whether transferred T cells migrate to any specific organ other than lymphoid organs. On 7 d after the transfer of GFP-T cells, T cell diminishment was observed in the spleen, LNs, and liver of B6/*lpr* recipient mice (Fig. 1D). The accumulation of the donor T cells was not observed in any specific organs such as the lung, pancreas, and kidney. Furthermore, the donor T cells did not accumulate in the thymus, bone marrow, and PBMCs of B6/*lpr* recipient mice (Fig. 1D). These findings demonstrate that transferred normal T cells fail to survive in the lymphoid organs such as the spleen and LNs of B6/*lpr* recipients.

Migratory response of normal T cells in Fas-deficient recipients

To examine the migration of normal T cells to lymphoid tissues, in vivo imaging analysis of the dynamics of normal T cells in B6 and B6/*lpr* mice was performed. At 30 min after the transfer of

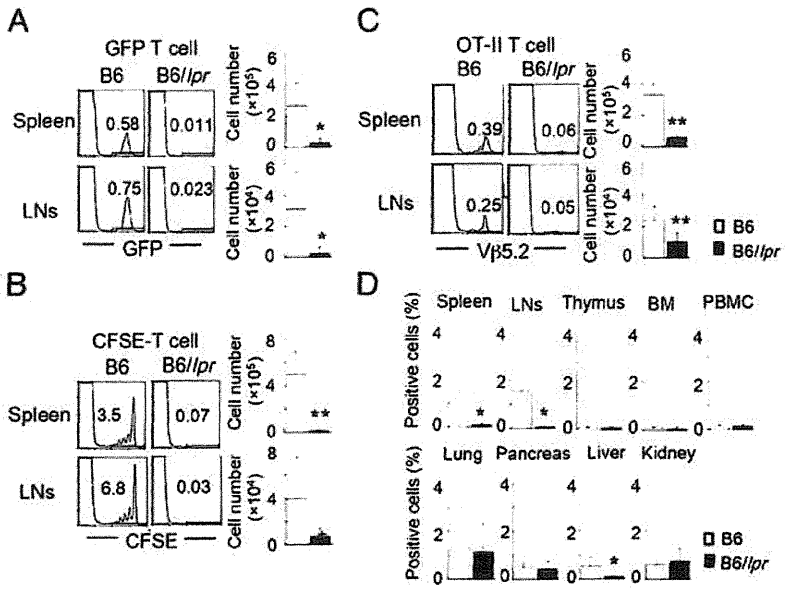

FIGURE 1. Dynamics of normal T cells in B6/*lpr* mice. **(A)** T cells (1×10^6) from GFP-TG mice were transferred into B6 and B6/*lpr* mice. GFP^+ T cells in the spleen and LNs of recipient mice at day 7 after the transfer were detected by flow cytometry. **(B)** CFSE-labeled T cells from B6 mice were transferred into irradiated (8.5 Gy) B6 and B6/*lpr* mice. $CFSE^+$ T cells in the spleen and LNs of recipient mice at day 7 after the transfer were detected by flow cytometry. **(C)** T cells (1×10^6) from OT-II mice were transferred into B6 and B6/*lpr* mice. Next day, OVA peptide was i.v. injected into the recipient mice. $V\beta5.2^+CD4^+$ T cells in the spleen and LNs of recipient mice at day 7 after the transfer were detected by flow cytometry. Cell numbers were compared between B6 and B6/*lpr* recipients ($n = 6$). **(D)** T cells from GFP-TG mice were transferred into B6 and B6/*lpr* mice. GFP^+ T cells in the spleen and LNs of recipient mice at day 7 after the transfer were detected by flow cytometry. GFP^+ cells (percentage) were shown as mean ± SD for five mice in each recipient group. $^*p < 0.05$, $^{**}p < 0.005$.

T cells, XenoLight DiR-labeled T cells were detected using an in vivo imaging analyzer. Although transferred T cells were detectable in the spleen of B6 and B6/*lpr* recipients, the fluorescence intensity in the spleen of B6/*lpr* recipients was considerably lower than that in the spleen of B6 recipients (Fig. 2A). This finding suggests that the transferred normal T cells were rapidly diminished in PBMCs before accumulating in lymphoid organs such as the spleen and LNs. In contrast, we have analyzed cell localization to the lung and liver after i.v. injection of T cells. Normal T cells were detectable in both *lpr* and control recipients, and there was no difference in T cell migration between *lpr* and control recipients (Supplemental Fig.1). Moreover, when the transferred T cells

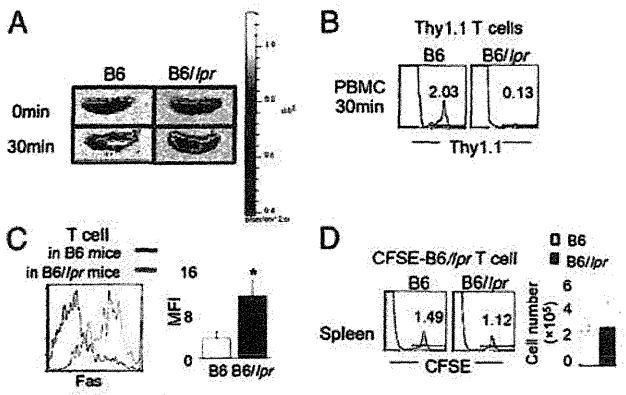

FIGURE 2. Rapid diminishment and Fas expression on the donor T cells in *lpr* recipients. **(A)** T cells (5×10^6) from B6 mice were labeled with XenoLight DiR and transferred into B6 and B6/*lpr* mice. The donor T cells in the spleen of the recipients 30 min after the transfer were detected using an in vivo imaging analyzer. Photos are representative of four mice in each recipient group. **(B)** T cells from B6 Thy1.1 mice were transferred into B6 and B6/*lpr* mice, and the donor T cells in PBMCs of the recipients 30 min after the transfer were detected by flow cytometry. Data are representative of five mice in each recipient group. **(C)** Cell surface Fas expression on the donor T cells in recipients was analyzed 30 min after the transfer by flow cytometry. Mean fluorescence intensity of Fas expression on donor T cells is shown as mean ± SD for five mice in each recipient group. $^*p < 0.05$. **(D)** CFSE-labeled T cells from B6/*lpr* mice were transferred into B6 and B6/*lpr* mice and detected at day 7 after transfer by flow cytometry. Data are representative of five mice in each recipient group.

($Thy1.1^+$) were analyzed 30 min after the transfer, the rapid diminishment of T cells in B6/*lpr* recipients had already been observed (Fig. 2B). This suggests that rapid death and clearance of normal T cells may have occurred in the B6/*lpr* recipients immediately after the transfer. Moreover, when the Fas expression on the transferred normal T cells in B6 or B6/*lpr* recipients was analyzed 30 min after the transfer, significantly increased Fas expression was observed on the T cells in B6/*lpr* recipients compared with those in B6 recipients (Fig. 2C). Furthermore, when CFSE-labeled T cells from B6/*lpr* mice were i.v. injected into B6 and B6/*lpr* mice, the T cell diminishment was not detectable in both recipient mice (Fig. 2D). These results suggest that Fas expression on normal T cells plays a crucial role in the induction of rapid T cells diminishment in Fas-deficient recipients. These results imply that Fas-mediated cell death of normal T cells is enhanced in a Fas-deficient immune environment.

FasL expression on immune cells in B6/lpr mice

Next, we analyzed FasL expression on peripheral immune cells in B6/*lpr* mice. When mRNA expression of FasL in the spleen of B6 and B6/*lpr* mice was analyzed by quantitative reverse transcription-PCR (RT-PCR), higher levels of FasL mRNA of all subsets including $CD4^+$ T cells, $CD8^+$ T cells, $B220^+$ B cells, $CD11c^+$ dendritic cells, and $CD11b^+$ macrophages were observed in B6/*lpr* mice compared with B6 mice (Fig. 3A). In addition, significantly increased FasL mRNA expression of subsets including $CD4^+$ T cells, $CD8^+$ T cells, and $CD11b^+$ macrophages was observed in PBMCs from B6/*lpr* mice compared with those of B6 mice (Fig. 3B). Therefore, we speculated that FasL–Fas-mediated apoptosis of normal T cells may be induced by the interaction with the peripheral immune cells in B6/*lpr* mice. In particular, because FasL mRNA expression on the $CD11b^+$ macrophages in the spleen and PBMCs of B6/*lpr* mice was much higher than that of B6 mice, macrophages may play a crucial role in T cell apoptosis and clearance in the immune system of B6/*lpr* mice. Thus, we focused on analyzing the macrophages in B6/*lpr* mice. When the surface expression of FasL on macrophages was analyzed by flow cytometry, the expression on the $CD11b^+$ macrophages of the PBMCs of B6/*lpr* mice was increased compared with that of B6 mice (Fig. 3C). These results suggest that increased FasL expressions on immune cells, including macrophages in a Fas-deficient immune condition, play an important

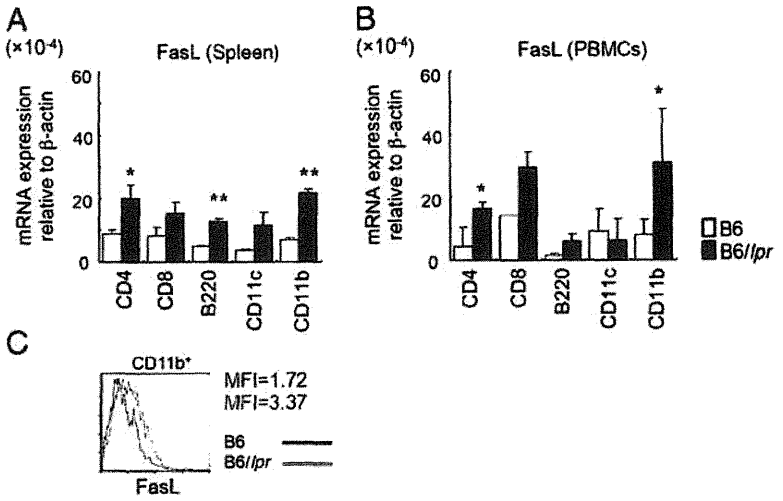

FIGURE 3. Enhanced expression of FasL on the immune cells in B6/*lpr* mice. (**A**) FasL mRNA expressions in spleen cells of B6 and B6/*lpr* mice were analyzed by quantitative RT-PCR. Data are shown as mean ± SD for five mice in each recipient group. $*p < 0.05$; $**p < 0.005$. (**B**) FasL mRNA expressions in PBMCs of B6 and B6/*lpr* mice were analyzed by quantitative RT-PCR. Data are shown as mean ± SD for five mice in each recipient group. $*p < 0.05$. (**C**) FasL expression on the CD11b$^+$ macrophages in PBMCs was detected by flow cytometry. Results are representative of three independent experiments.

role in the Fas-mediated rapid death of normal T cells in B6/*lpr* mice.

*Functions of macrophages in B6/*lpr *mice*

To understand the functions of the peripheral macrophages in B6/*lpr* mice, macrophages from thioglycolate-elicited PECs were used for analyzing their interaction with normal T cells. When the expression level of FasL on PECs was analyzed, significantly increased expression of FasL on PECs from B6/*lpr* mice was detected compared with B6 mice (Fig. 4A). Next, we examined whether in vitro T cell death was induced by coculture with PECs from B6/*lpr* mice. The proportion of apoptotic T cells cocultured with B6/*lpr* PECs was significantly enhanced compared with that of normal T cells cocultured with B6 PECs (Fig. 4B). To determine whether B6/*lpr* PECs engulf dead T cells rapidly, CFSE-labeled normal T cells were cocultured with CD11b$^+$ PECs for 3 h, and CD11b$^+$CFSE$^+$ macrophages engulfing apoptotic T cells were analyzed. We detected a significant increase of CFSE$^+$ CD11b$^+$ macrophages in B6/*lpr* mice compared with B6 mice (Fig. 4C). In addition, we investigated the phagocytic activity of B6/*lpr* macrophages with FITC-labeled latex beads. The phagocytic activity of CD11b$^+$ PECs in B6/*lpr* mice was significantly increased compared with that in B6 mice (Fig. 4D). To rule out that the apoptotic cells attached to macrophages, we fixed the macrophages after phagocytosis assay and then treated them with 0.01% Triton X-100. Because there was no change in the proportion of CD11b$^+$FITC$^+$ macrophages between before and after Triton X treatment, the macrophages engulfed, but not bound to, the beads in this assay (Supplemental Fig. 2). These results suggest that enhanced FasL expression on the macrophages in B6/*lpr* mice triggers the rapid cell death of normal T cells in a Fas-deficient immune environment, and increased phagocytic activity of B6/*lpr* macrophages plays a key role in the clearance of dead T cells.

In vivo functions of Fas-deficient macrophages

To determine the in vivo functions of macrophages in B6/*lpr* mice, normal T cells from GFP-TG mice were i.p. injected into the recipient mice that had been injected with thioglycolate. At 6 h after T cell injection, PECs including injected T cells were analyzed. Consistent with the results obtained from the i.v. injection of normal T cells into B6/*lpr* mice, the T cells injected (i.p.) into B6/*lpr* mice were significantly decreased compared with those injected into B6 mice (Fig. 5A). The number of apoptotic cells showing Annexin V$^+$ of injected T cells in B6/*lpr* mice was significantly higher compared with that in B6 mice (Fig. 5B). The depletion of T cells in B6/*lpr* recipients was inhibited by i.p. injection of anti-FasL mAb (Fig. 5C). Furthermore, when normal

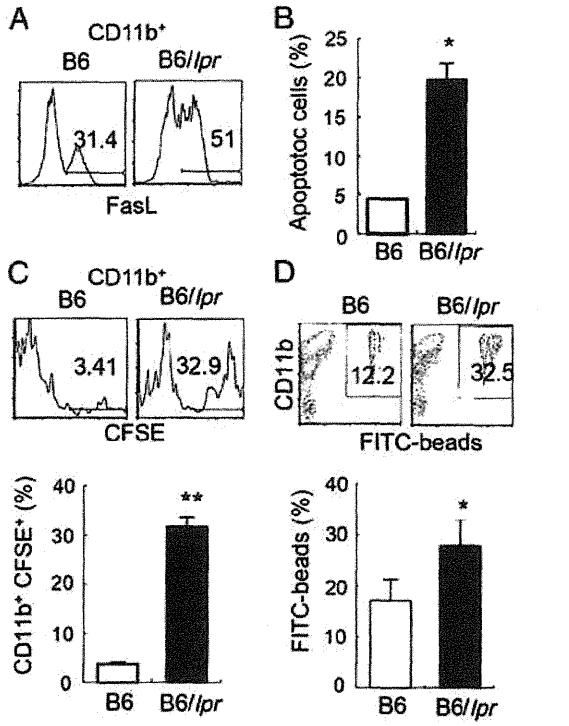

FIGURE 4. Enhanced FasL expression and phagocytotic activity of *lpr* macrophages in vitro. B6 and B6/*lpr* mice were i.p. injected with thioglycolate to obtain PECs. On day 4 after the injection, PECs were collected from peritoneal cavity. (**A**) FasL expression on CD11b$^+$ macrophages in PECs of B6 and B6/*lpr* mice was analyzed by flow cytometry. Data are representative of four independent experiments. (**B**) CFSE-labeled T cells from Thy1.1 B6 mice were cocultured with the CD11b$^+$ macrophages from PECs of B6 and B6/*lpr* mice. Annexin V$^+$ apoptotic T cells (percentage) are shown as mean ± SD for five mice in each group. $*p < 0.05$. (**C**) CFSE-labeled T cells from B6 mice were cocultured with the CD11b$^+$ macrophages from PECs of B6 and B6/*lpr* mice. Phagocytosis of CFSE$^+$ T cells by the CD11b$^+$ cells in PECs was evaluated by flow cytometry. Results are shown as mean ± SD for five mice in each group. $**p < 0.005$. (**D**) Phagocytic activity of CD11b$^+$ macrophages in PECs was evaluated by uptake of FITC-conjugated beads in vitro. Results are shown as mean ± SD for five mice in each group. $**p < 0.005$.

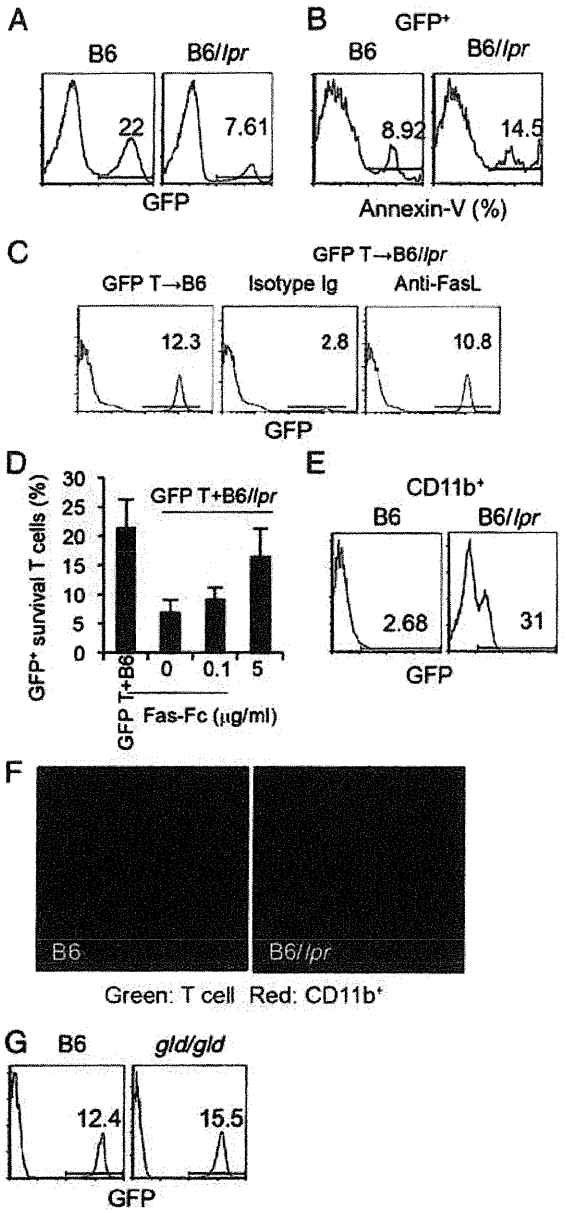

FIGURE 5. In vivo rapid death and phagocytosis of T cells by macrophages. **(A)** T cells (1×10^6) from GFP-TG mice were i.p. injected into the recipient mice treated with thioglycolate. GFP^+ T cells in PECs were detected by flow cytometry. Data are representative of four mice in each recipient group. **(B)** Annexin V^+ apoptotic cells (percentage) of GFP^+ T cells in PECs were detected by flow cytometry. Data are representative of four mice in each recipient group. **(C)** GFP T cells (1×10^6) were i.p. injected into thioglycolate-treated B6/*lpr* recipients together with anti-Fas mAb or isotype control Ig. **(D)** GFP T cells (5×10^4) were cocultured with B6/*lpr* PECs (2×10^5) fro 24 h in vitro in the presence of Fas-Fc fusion protein (0, 0.1, and 5 μg/ml). GFP^+ survival cells are shown as mean ± SD for triplicates. **(E)** Phagocytosis of GFP^+ T cells by the $CD11b^+$ macrophages in PECs was evaluated by flow cytometry. Data are representative of four mice in each recipient group. **(F)** GFP^+ T cells (green) and $CD11b^+$ macrophages (red) in PECs were detected by confocal microscopy. Original magnification ×630. Data are representative of four three independent experiments. **(G)** T cells from GFP-TG mice were i.p. injected into B6 and B6/*gld* mice treated with thioglycolate. GFP^+ T cells in PECs were detected by flow cytometry. Data are representative of four mice in each recipient group.

GFP-T cells were i.p. transferred into B6/*lpr* mice together with Fas-Fc fusion protein (0.1 and 5 μg/ml), survival T cells were significantly increased in comparison with those of the recipients without Fas-Fc (Fig. 5D). In addition, the phagocytic activity of $CD11b^+$ PECs in B6/*lpr* was significantly enhanced compared with that in B6/mice (Fig. 5E). Furthermore, microscopic analysis showed fewer normal T cells (GFP^+) in B6/*lpr* mice compared with B6 mice: moreover, it revealed phagocytic fragments of GFP^+ T cells within the macrophages in B6/*lpr* mice, although the fragments within the macrophages in B6 mice were undetectable (Fig. 5F). In contrast, when normal T cells from GFP-TG mice were i.p. injected into B6 and B6/*gld* mice, which are deficient in FasL expression, T cell diminishment was not observed (Fig. 5G). In contrast, we have performed the experiment using purified B cells. Because deletion of normal B cells in *lpr* recipients was not observed (Supplemental Fig. 3), T cell apoptosis may be closely associated with phagocytosis of *lpr* macrophages. Our findings reveal that Fas-deficient macrophages can induce rapid apoptosis through upregulated FasL and that Fas-deficient macrophages rapidly engulf apoptotic T cells.

Enhanced activation of Fas-deficient macrophages through NF-κB

NF-κB signaling plays a crucial role in the activation of macrophages (22, 23). Phosphorylation of IκBα, an endogenous inhibitory molecule of NF-κB activation by the interaction with NF-κB subunits, in $CD11b^+$PECs from B6/*lpr* mice was much higher than that in $CD11b^+$ PECs from B6 mice (Fig. 6A). Moreover, nuclear transport of NF-κB subunits such as p50 and p65 in $CD11b^+$ PECs from B6/*lpr* mice was significantly enhanced compared with that in $CD11b^+$ PECs from B6 mice (Fig. 6A). In addition, the transcriptional activity of NF-κB in the nuclear protein of the $CD11b^+$ PECs from B6/*lpr* mice was significantly increased compared with that from B6 mice (Fig. 6B). In immune cells, including macrophages, there are several genes regulated by NF-κB such as TNF-α, IL-6, IL-1β, and FasL in immune cells including macrophage (24–27). The mRNA expression of TNF-α, IL-6, and IL-1β in $CD11b^+$ PECs from B6/*lpr* mice was not increased compared with that from B6 mice (Fig. 6C). In contrast, the FasL mRNA level in the $CD11b^+$ PECs from B6/*lpr* mice was significantly higher than that from B6 mice (Fig. 6D). When FasL mRNA of the $CD11b^+$ PECs from $NF\text{-}\kappa B_1$ gene knockout mice bearing a *fas* gene mutant ($NF\text{-}\kappa B_1^{-/-}$/*lpr*) was analyzed, the expression level was similar to that of B6 mice (Fig. 6D). Furthermore, the diminishment of normal T cells in $NF\text{-}\kappa B_1^{-/-}$/*lpr* mice was not observed (Fig. 6E, 6F). These results suggest that FasL overexpression through NF-κB activation of macrophages is important for rapid T cell death in a Fas-deficient immune system.

Alteration of Fas expression on normal T cells in a Fas-deficient immune system

Fas expression is regulated by several factors or signaling pathways (28–31). One potent factor that induces Fas expression is IFN-γ (28). When the serum level of IFN-γ was analyzed by ELISA, we found that the concentration of the sera in B6/*lpr* mice was significantly higher compared with that in B6 mice (Fig. 7A). To determine the source of the high level of IFN-γ, subsets of peripheral immune cells including $CD4^+$ T cells, $CD8^+$ T cells, $CD11b^+$ macrophages, $CD11c^+$ dendritic cells, and $B220^+$ B cells in PBMCs were purified, and IFN-γ mRNA was analyzed by quantitative RT-PCR. The mRNA levels in $CD4^+$, $CD8^+$ T, and $B220^+$ B cells from B6/*lpr* mice increased significantly compared with those in B6 mice (Fig. 7B). When the T cells from normal mice or $IFN\gamma R^{-/-}$ mice were labeled with CFSE and were i.v. injected into B6/*lpr* mice, Fas expression on T cells in $IFN\gamma R^{-/-}$ mice was not enhanced, although the expression on T cells from B6 mice was considerably increased in Fas-deficient recipients

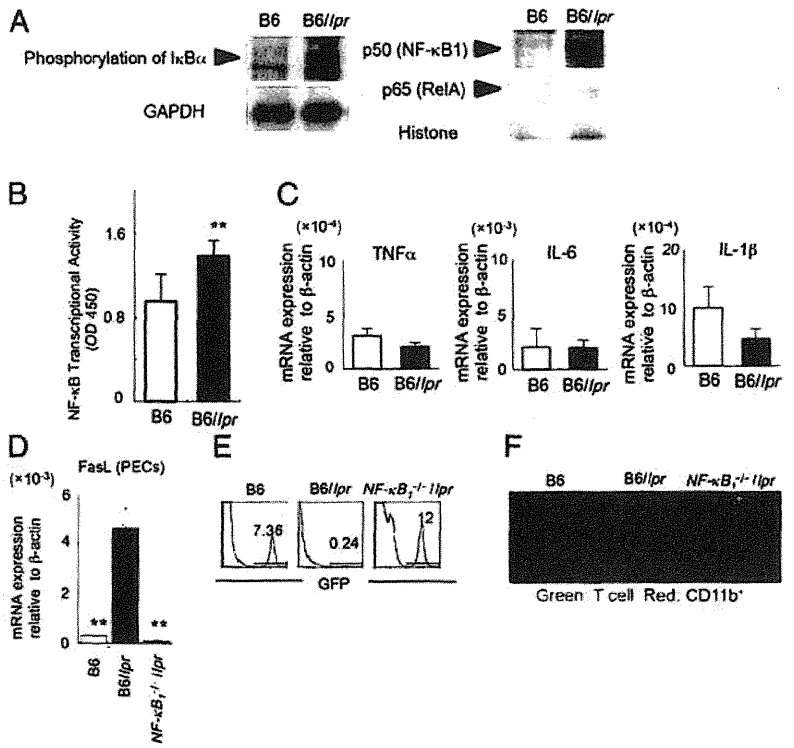

FIGURE 6. Control of FasL expression on *lpr* macrophages by NF-κB activation. (**A**) Phosphorylation of IκBα and nuclear translocation of the NF-κB subunits of CD11b$^+$ macrophages from thioglycolate-induced PECs were analyzed by Western blotting. GAPDH and histones were used as housekeeping proteins. Data are representative of three independent experiments. (**B**) Transcriptional activity of NF-κB in B6 and B6/*lpr* macrophages was detected. Results are shown as mean ± SD for five mice in each group. $^{**}p < 0.005$. (**C**) The mRNA expression of NF-κB–target genes was analyzed by quantitative RT-PCR. Data are shown as mean ± SD for five mice in each group. (**D**) FasL mRNA expression in the CD11b$^+$ macrophages from thioglycolate-induced PECs in B6, B6/*lpr*, and *NF-κB1*$^{-/-}$/*lpr* mice was analyzed by quantitative RT-PCR. Data are shown as mean ± SD for five mice in each group. $^{**}p < 0.005$. (**E**) T cells from GFP-TG mice were i.p. injected into B6, B6/*lpr*, and *NF-κB1*$^{-/-}$/*lpr* mice pretreated with thioglycolate. GFP$^+$ T cells in PECs were detected by flow cytometry. Data are representative of five mice in each group. (**F**) GFP$^+$ T cells (green) and CD11b$^+$ macrophages (red) in PECs were detected by confocal microscopy. Original magnification ×630. Photos are representative of four independent experiments.

(Fig. 7C). Fas expression on T cells was enhanced by recombinant IFN-γ in a dose-dependent manner (Supplemental Fig. 4). In addition, when T cells from *IFNγR*$^{-/-}$ mice were i.v. injected into B6/*lpr* mice, T cell diminishment, which had been observed in the Fas-deficient recipients, was not detectable (Fig. 7D). Moreover, when T cells from *IFNγR*$^{-/-}$ mice were cocultured with *lpr* PECs, survival T cells of *IFNγR*$^{-/-}$ mice were significantly increased compared with those of wild-type mice (Fig. 7E). By the

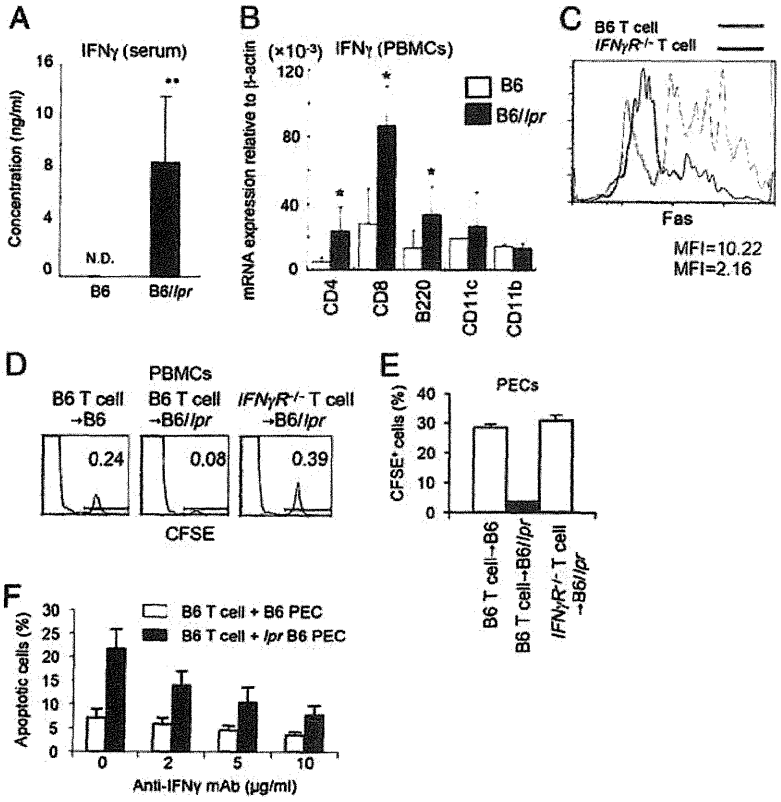

FIGURE 7. Regulation of Fas expression on donor T cells by IFN-γ in *lpr* mice. (**A**) Concentration of IFN-γ in the sera of B6 and B6/*lpr* mice was measured by ELISA. Results are shown as mean ± SD for six mice in each group. $^{**}p < 0.005$. (**B**) IFN-γ mRNA expressions in the subsets of spleen cells from B6 and B6/*lpr* mice were analyzed by quantitative RT-PCR. Results are shown as mean ± SD for five mice in each group. $^{*}p < 0.05$. (**C**) CFSE-labeled T cells from B6 and *IFNγR*$^{-/-}$ mice were i.v. injected into B6/*lpr* mice. Fas expression on the donor T cells in PBMCs of recipients was analyzed by flow cytometry. Data are representative of five mice in each group. Gray shadow shows isotype negative control. (**D**) CFSE-labeled T cells from B6 and *IFNγR*$^{-/-}$ mice were i.v. injected into B6 or B6/*lpr* mice and were detected by flow cytometry. Data are representative of four mice in each group. (**E**) CFSE-labeled T cells from B6 and *IFNγR*$^{-/-}$ mice were i.p. injected into thioglicolate-treated B6 or B6/*lpr* mice. CFSE$^+$ T cells in PECs were analyzed by flow cytometry. Results are shown as mean ± SD for four mice in each group. (**F**) T cells (2×10^4) from B6 mice were cocultured for 8 h with B6 or B6/*lpr* PECs (1×10^5) in the presence of anti–IFN-γ mAb (0, 2, 5, and 10 μg/ml). Apoptotic T cells were evaluated by flow cytometric analysis of expression of Annexin V. Results are shown as mean ± SD for triplicates in each group.

pretreatment of anti–IFN-γ mAb, apoptosis of normal activated T cell interacted with *lpr* PECs was inhibited in the dose-dependent manner (Fig. 7F). These findings suggest that the high level of IFN-γ in B6/*lpr* mice enhances Fas expression on injected normal T cells and that immune cells in B6/*lpr* mice highly expressing FasL induce Fas-mediated and rapid apoptosis of T cells.

Discussion

In this study, we confirmed that normal T cells failed to survive in a Fas-deficient immune condition using the transfer experiments. In addition, the homeostatic proliferation of T cells in lymphopenic recipients of *lpr* mice and Ag-specific T cell response in *lpr* mice were not observed. These findings are consistent with the results in the previous reports regarding the failure of normal lymphocyte survival in *lpr* hosts (17, 18). The phenomenon was thought to occur because of the induction of T cell apoptosis in *lpr* recipients because the transferred T cells did not migrate in any specific organs other than lymphoid tissues and the liver.

Because the diminishment of normal T cells was observed in PBMCs in 30 min immediately after the transfer, rapid death of transferred T cells may have occurred in *lpr* recipients. However, T cell diminishment in *lpr* donor mice was undetectable. Thus, the rapid T cell death occurred by the presence or absence of the Fas molecule on these cells.

Although enhanced FasL expression on immune cells in *lpr* mice has been described previously (18, 20), it was unclear as to which subset of immune cells in *lpr* mice overexpressed FasL molecule. In this study, mRNA expression of FasL of all subsets in the spleen and PBMCs of *lpr* mice was significantly higher than that of control mice. In particular, FasL mRNA expression in $CD11b^+$ macrophages in *lpr* mice was significantly increased compared with that in control mice. In addition, when thioglycolate-elicited PECs, including a number of macrophages, were used to analyze the interaction with T cell in vivo and in vitro, enhanced rapid death and clearance of T cells by *lpr* macrophages was observed. Furthermore, phagocytic activity of *lpr* macrophages was considerably enhanced compared with control macrophages. These results suggest that *lpr* macrophages can phagocyte apoptotic T cells promptly as well as induce the rapid T cell death in the periphery. The *lpr* macrophages with enhanced expression of FasL may induce rapid death of T cells and promptly engulf the apoptotic cells by FasL-independent phagocytosis. There may be unknown cellular mechanism like "Eat me signal."

FasL, a type II transmembrane protein belonging to the TNF superfamily, is a well-characterized apoptosis initiating protein (32–34). Some transcription factors have been shown to regulate FasL gene expression, including specificity protein-1, IFN regulatory factor-1, NF in activated T cells and NF-κB (35–37). NF-κB plays key roles in differentiation and activation of macrophages (22, 38). Our results suggest that the direct contribution of macrophages to the induction of rapid death of T cells is very important for effective phagocytosis of apoptotic T cells. Furthermore, our results imply that the induction of expression of FasL in macrophages by NF-κB is negatively controlled by Fas signaling. This is related to our previous report that Fas signaling controls RANKL signaling following NF-κB activation in dendritic cells (39). Fas signaling may play important roles in NF-κB activation in relation to cell activation, survival, and growth in addition to apoptosis.

As to the relationship between FasL expression and phagocytosis in macrophages, it was reported that enhanced expression of FasL on Kupffer cells is associated with phagocytosis of apoptotic T cells in human liver allografts (40). Although further experiments will be needed to confirm the cellular mechanism, FasL-enhanced macrophages may engulf apoptotic cells effectively.

It is widely established that Fas expression on peripheral T cells plays a key role in AICD to maintain peripheral immune system (2, 3, 5). Fas expression on T cells increases by TCR signaling (41). In addition, some cytokines such as IL-2 and/or IFN-γ trigger the enhancement of Fas expression on T cells (42). Our results imply that an extremely high concentration of IFN-γ in the serum of *lpr* mice acts on the induction of Fas expression on the transferred T cells directly. When T cells from IFN-γR knockout mice were transferred into *lpr* mice, the rapid death and diminishment of T cells was not observed. These results strongly suggest that Fas expression on peripheral T cells is controlled through the IFN-γ/IFN-γR.

With regard to the control of the Fas expression of cells other than the T cell, it was reported that TNF-α can control the expression of fibroblasts in addition to IFN-γ (30). Although we found a high concentration of IFN-γ in the serum from *lpr* mice, the level of TNF-α concentration in the serum from *lpr* mice was similar to that from control mice (data not shown). In this study, when naive T cells from normal mice were transferred, they were not activated and slightly expressed the Fas molecule on the cell surface. Because of the exposure to the high concentration of IFN-γ in *lpr* mice, Fas expression on T cells rapidly increased. The immune cells highly expressing FasL including macrophages of *lpr* mice may induce the rapid apoptosis of T cells, and the macrophages in the peripheral immune system may rapidly phagocytize the apoptotic T cells.

In contrast, many reports indicate that B cells are maintained by Fas and Bim-dependent apoptosis to protect autoimmunity (43–45). In our experiment, $CD19^+$ B cells failed to undergo apoptosis in Fas-deficient host, although FasL expression on immune cells was enhanced. This finding implies that rapid T cell death may be triggered by cell–cell contact between normal T cells and Fas-deficient macrophages through the interaction with cell surface molecules such as MHC class II, costimulatory molecules, or TCR, although its precise mechanism has been still clarified.

Our results suggest that Fas signaling contributes to nonapoptotic functions such as the phagocytic activity of macrophages. Fas promotes the differentiation, proliferation, and maturation in several cells (1, 2, 46). Fas-associated death domain–mediated activation of caspase 8 is essential for the process of apoptosis of various cells (12, 47). In addition, it was reported that Rho GTPase Rac1 sensitizes T cells to Fas-induced apoptosis correlated with Rac-mediated cytoskeletal reorganization, dephosphorylation of the ezrin/radixin/moesin family of cytoskeletal linker proteins, and the translocation of Fas to lipid raft microdomain (48). However, the molecular mechanism for controlling the phagocytic activity of macrophages through Fas signaling has yet to be elucidated.

Although it has been reported that normal immune cells failed to survive in *lpr* recipients, the precise mechanism for its phenomenon remained unclear. In this study, we found that abnormal macrophages in *lpr* mice play critical roles in the disorder of the peripheral immune system. Our findings are thought to be important for therapeutic strategies for immune disorders such as ALPS or the other autoimmune diseases related to the abnormal expression of Fas on immune cells. In addition, this study suggests that Fas expression on macrophages contributes to the survival of T cells in the peripheral immune system. Taken together, this study strongly suggests that Fas-expressing macrophages play a pivotal role in maintaining T cell homeostasis in addition to AICD in the periphery.

Acknowledgments

We thank S. Katada, A. Katayama, and N. Kino for technical assistance.

Disclosures

The authors have no financial conflicts of interest.

References

1. Nagata, S. 1997. Apoptosis by death factor. *Cell* 88: 355–365.
2. Krammer, P. H. 2000. CD95's deadly mission in the immune system. *Nature* 407: 789–795.
3. Strasser, A., P. J. Jost, and S. Nagata. 2009. The many roles of FAS receptor signaling in the immune system. *Immunity* 30: 180–192.
4. Alderson, M. R., T. W. Tough, T. Davis-Smith, S. Braddy, B. Falk, K. A. Schooley, R. G. Goodwin, C. A. Smith, F. Ramsdell, and D. H. Lynch. 1995. Fas ligand mediates activation-induced cell death in human T lymphocytes. *J. Exp. Med.* 181: 71–77.
5. Maher, S., D. Toomey, C. Condron, and D. Bouchier-Hayes. 2002. Activation-induced cell death: the controversial role of Fas and Fas ligand in immune privilege and tumour counterattack. *Immunol. Cell Biol.* 80: 131–137.
6. Zhang, J., X. Xu, and Y. Liu. 2004. Activation-induced cell death in T cells and autoimmunity. *Cell. Mol. Immunol.* 1: 186–192.
7. Shultz, L. D., and C. L. Sidman. 1987. Genetically determined murine models of immunodeficiency. *Annu. Rev. Immunol.* 5: 367–403.
8. Jabs, D. A., and R. A. Prendergast. 1988. Murine models of Sjögren's syndrome: immunohistologic analysis of different strains. *Invest. Ophthalmol. Vis. Sci.* 29: 1437–1443.
9. Cohen, P. L., and R. A. Eisenberg. 1991. Lpr and gld: single gene models of systemic autoimmunity and lymphoproliferative disease. *Annu. Rev. Immunol.* 9: 243–269.
10. Kotzin, B. L. 1996. Systemic lupus erythematosus. *Cell* 85: 303–306.
11. Singer, P. A., and A. N. Theofilopoulos. 1990. Novel origin of lpr and gld cells and possible implications in autoimmunity. *J. Autoimmun.* 3: 123–135.
12. Boldin, M. P., E. E. Varfolomeev, Z. Pancer, I. L. Mett, J. H. Camonis, and D. Wallach. 1995. A novel protein that interacts with the death domain of Fas/APO1 contains a sequence motif related to the death domain. *J. Biol. Chem.* 270: 7795–7798.
13. Scaffidi, C., S. Fulda, A. Srinivasan, C. Friesen, F. Li, K. J. Tomaselli, K. M. Debatin, P. H. Krammer, and M. E. Peter. 1998. Two CD95 (APO-1/Fas) signaling pathways. *EMBO J.* 17: 1675–1687.
14. Curtin, J. F., and T. G. Cotter. 2003. Live and let die: regulatory mechanisms in Fas-mediated apoptosis. *Cell. Signal.* 15: 983–992.
15. Hughes, P. D., G. T. Belz, K. A. Fortner, R. C. Budd, A. Strasser, and P. Bouillet. 2008. Apoptosis receptors Fas and Bim coorerate I shutdown of chronic immune receptors and prevention of autoimmunity. *Immunity* 28: 197–205.
16. Green, D. R., and M. Schuler. 2000. T cell development: some cells get all the breaks. *Nat. Immunol.* 1: 15–17.
17. Ettinger, R., J. K. Wang, P. Bossu, K. Papas, C. L. Sidman, A. K. Abbas, and A. Marshak-Rothstein. 1994. Functional distinctions between MRL-lpr and MRL-gld lymphocytes: normal cells reverse the gld but not lpr immunoregulatory defect. *J. Immunol.* 152: 1557–1568.
18. Wei, Y., K. Chen, G. C. Sharp, and H. Braley-Mullen. 2004. Fas ligand is required for resolution of granulomatous experimental autoimmune thyroiditis. *J. Immunol.* 173: 7615–7621.
19. Theofilopoulos, A. N., R. S. Balderas, Y. Gozes, M. T. Aguado, L. M. Hang, P. R. Morrow, and F. J. Dixon. 1985. Association of lpr gene with graft-vs.-host disease-like syndrome. *J. Exp. Med.* 162: 1–18.
20. Chu, J. L., P. Ramos, A. Rosendorff, J. Nikolić-Zugić, E. Lacy, A. Matsuzawa, and K. B. Elkon. 1995. Massive upregulation of the Fas ligand in lpr and gld mice: implications for Fas regulation and the graft-versus-host disease-like wasting syndrome. *J. Exp. Med.* 181: 393–398.
21. Allison, J., and A. Strasser. 1998. Mechanisms of β cell death in diabetes: a minor role for CD95. *Proc. Natl. Acad. Sci. USA* 95: 13818–13822.
22. Hawiger, J. 2001. Innate immunity and inflammation: a transcriptional paradigm. *Immunol. Res.* 23: 99–109.
23. Spehlmann, M. E., and L. Eckmann. 2009. Nuclear factor-κB in intestinal protection and destruction. *Curr. Opin. Gastroenterol.* 25: 92–99.
24. Dunn, S. M., L. S. Coles, R. K. Lang, S. Gerondakis, M. A. Vadas, and M. F. Shannon. 1994. Requirement for nuclear factor (NF)-κB p65 and NF-interleukin-6 binding elements in the tumor necrosis factor response region of the granulocyte colony-stimulating factor promoter. *Blood* 83: 2469–2479.
25. Baer, M., A. Dillner, R. C. Schwartz, C. Sedon, S. Nedospasov, and P. F. Johnson. 1998. Tumor necrosis factor α transcription in macrophages is attenuated by an autocrine factor that preferentially induces NF-κB p50. *Mol. Cell. Biol.* 18: 5678–5689.
26. Mercurio, F., and A. M. Manning. 1999. Multiple signals converging on NF-κB. *Curr. Opin. Cell Biol.* 11: 226–232.
27. Torgler, R., S. Jakob, E. Ontsouka, U. Nachbur, C. Mueller, D. R. Green, and T. Brunner. 2004. Regulation of activation-induced Fas (CD95/Apo-1) ligand expression in T cells by the cyclin B1/Cdk1 complex. *J. Biol. Chem.* 279: 37334–37342.
28. Nagafuji, K., T. Shibuya, M. Harada, S. Mizuno, K. Takenaka, T. Miyamoto, T. Okamura, H. Gondo, and Y. Niho. 1995. Functional expression of Fas antigen (CD95) on hematopoietic progenitor cells. *Blood* 86: 883–889.
29. De Maria, R., and R. Testi. 1998. Fas-FasL interactions: a common pathogenetic mechanism in organ-specific autoimmunity. *Immunol. Today* 19: 121–125.
30. Frankel, S. K., G. P. Cosgrove, S. I. Cha, C. D. Cool, M. W. Wynes, B. L. Edelman, K. K. Brown, and D. W. Riches. 2006. TNF-α sensitizes normal and fibrotic human lung fibroblasts to Fas-induced apoptosis. *Am. J. Respir. Cell Mol. Biol.* 34: 293–304.
31. Wynes, M. W., B. L. Edelman, A. G. Kostyk, M. G. Edwards, C. Coldren, S. D. Groshong, G. P. Cosgrove, E. F. Redente, A. Bamberg, K. K. Brown, et al. 2011. Increased cell surface Fas expression is necessary and sufficient to sensitize lung fibroblasts to Fas ligation-induced apoptosis: implications for fibroblast accumulation in idiopathic pulmonary fibrosis. *J. Immunol.* 187: 527–537.
32. Ju, S. T., D. J. Panka, H. Cui, R. Ettinger, M. el-Khatib, D. H. Sherr, B. Z. Stanger, and A. Marshak-Rothstein. 1995. Fas(CD95)/FasL interactions required for programmed cell death after T-cell activation. *Nature* 373: 444–448.
33. Janssen, O., J. Qian, A. Linkermann, and D. Kabelitz. 2003. CD95 ligand—death factor and costimulatory molecule? *Cell Death Differ.* 10: 1215–1225.
34. Lettau, M., M. Paulsen, H. Schmidt, and O. Janssen. 2011. Insights into the molecular regulation of FasL (CD178) biology. *Eur. J. Cell Biol.* 90: 456–466.
35. Chow, W. A., J. J. Fang, and J. K. Yee. 2000. The IFN regulatory factor family participates in regulation of Fas ligand gene expression in T cells. *J. Immunol.* 164: 3512–3518.
36. Jayanthi, S., X. Deng, B. Ladenheim, M. T. McCoy, A. Cluster, N. S. Cai, and J. L. Cadet. 2005. Calcineurin/NFAT-induced up-regulation of the Fas ligand/Fas death pathway is involved in methamphetamine-induced neuronal apoptosis. *Proc. Natl. Acad. Sci. USA* 102: 868–873.
37. Yao, P. L., Y. C. Lin, P. Sawhney, and J. H. Richburg. 2007. Transcriptional regulation of FasL expression and participation of sTNF-α in response to sertoli cell injury. *J. Biol. Chem.* 282: 5420–5431.
38. Lawrence, T., and G. Natoli. 2011. Transcriptional regulation of macrophage polarization: enabling diversity with identity. *Nat. Rev. Immunol.* 11: 750–761.
39. Izawa, T., N. Ishimaru, K. Moriyama, M. Kohashi, R. Arakaki, and Y. Hayashi. 2007. Crosstalk between RANKL and Fas signaling in dendritic cells controls immune tolerance. *Blood* 110: 242–250.
40. Miyagawa-Hayashino, A., T. Tsuruyama, H. Egawa, H. Haga, H. Sakashita, T. Okuno, S. Toyokuni, K. Tamaki, H. Yamabe, T. Manabe, and S. Uemoto. 2007. FasL expression I hepatic antigen-presenting cells and phagocytosis of apoptotic T cells by FasL$^+$ kupffer cells are indicators of rejection activity in human liver allografts. *Am. J. Pathol.* 177: 1499–1508.
41. Marrack, P., and J. Kappler. 2004. Control of T cell viability. *Annu. Rev. Immunol.* 22: 765–787.
42. Carter, L. L., X. Zhang, C. Dubey, P. Rogers, L. Tsui, and S. L. Swain. 1998. Regulation of T cell subsets from naive to memory. *J. Immunother.* 21: 181–187.
43. Hutcheson, J., J. C. Scatizzi, A. M. Siddiqui, G. K. Haines, III, T. Wu, Q. Z. Li, L. S. Davis, C. Mohan, and H. Perlman. 2008. Combined deficiency of proapoptotic regulators Bim and Fas results in the early onset of systemic autoimmunity. *Immunity* 28: 206–217.
44. Bouillet, P., D. Metcalf, D. C. Huang, D. M. Tarlinton, T. W. Kay, F. Köntgen, J. M. Adams, and A. Strasser. 1999. Proapoptotic Bcl-2 relative Bim required for certain apoptotic responses, leukocyte homeostasis, and to preclude autoimmunity. *Science* 286: 1735–1738.
45. Enders, A., P. Bouillet, H. Puthalakath, Y. Xu, D. M. Tarlinton, and A. Strasser. 2003. Loss of the pro-apoptotic BH3-only Bcl-2 family member Bim inhibits BCR stimulation-induced apoptosis and deletion of autoreactive B cells. *J. Exp. Med.* 198: 1119–1126.
46. Peter, M. E., R. C. Budd, J. Desbarats, S. M. Hedrick, A. O. Hueber, M. K. Newell, L. B. Owen, R. M. Pope, J. Tschopp, H. Wajant, et al. 2007. The CD95 receptor: apoptosis revisited. *Cell* 129: 447–450.
47. Muzio, M., A. M. Chinnaiyan, F. C. Kischkel, K. O'Rourke, A. Shevchenko, J. Ni, C. Scaffidi, J. D. Bretz, M. Zhang, R. Gentz, et al. 1996. FLICE, a novel FADD-homologous ICE/CED-3-like protease, is recruited to the CD95 (Fas/APO-1) death—inducing signaling complex. *Cell* 85: 817–827.
48. Ramaswamy, M., C. Dumont, A. C. Cruz, J. R. Muppidi, T. S. Gomez, D. D. Billadeau, V. L. Tybulewicz, and R. M. Siegel. 2007. Cutting edge: Rac GTPases sensitize activated T cells to die via Fas. *J. Immunol.* 179: 6384–6388.

The American Journal of Pathology, Vol. 180, No. 1, January 2012

DOI: 10.1016/j.ajpath.2011.09.027

Immunopathology and Infectious Diseases

CCR7 with $S1P_1$ Signaling through AP-1 for Migration of $Foxp3^+$ Regulatory T-Cells Controls Autoimmune Exocrinopathy

Naozumi Ishimaru,* Akiko Yamada,* Takeshi Nitta,† Rieko Arakaki,* Martin Lipp,‡ Yousuke Takahama,† and Yoshio Hayashi*

From the Department of Oral Molecular Pathology, Institute of Health Biosciences, The University of Tokushima Graduate School, Tokushima, Japan; the Department of Experimental Immunology,† Institute for Genome Research, The University of Tokushima, Tokushima, Japan; and the Department of Molecular Tumor Genetics and Immunogenetics,‡ Max-Delbruck Center for Molecular Medicine, Berlin, Germany*

Forkhead box p3-positive ($Foxp3^+$) regulatory T cells (T_{reg} cells) participate in maintaining peripheral immune tolerance and suppressing autoimmunity. We recently reported that *in situ* patrolling by C-C-chemokine receptor 7 ($CCR7)^+$ T_{reg} cells in target organs is essential for controlling autoimmune lesions in Sjögren's syndrome. In the present study, the molecular mechanism underlying CCR7-mediated T_{reg} cell migration was investigated in a mouse model. The impaired migratory response of $Ccr7^{-/-}$ T_{reg} cells to sphingosine 1-phosphate (S1P) occurred because of defective association of S1P receptor 1 ($S1P_1$) with a G coupled–protein. In addition, T-cell receptor (TCR)- and $S1P_1$-mediated Ras-related C3 botulinum toxin substrate 1 (Rac-1), extracellular signal-related kinase (ERK), and c-Jun phosphorylation required for activator protein 1 (AP-1) transcriptional activity were significantly impaired in $Ccr7^{-/-}$ T_{reg} cells. Surprisingly, the abnormal nuclear localization of Foxp3 was detected after abrogation of the c-Jun and Foxp3 interaction in the nucleus of $Ccr7^{-/-}$ T_{reg} cells. These results indicate that CCR7 essentially controls the migratory function of T_{reg} cells through $S1P_1$-mediated AP-1 signaling, which is regulated through its interaction with Foxp3 in the nucleus. *(Am J Pathol 2012, 180: 199–208; DOI: 10.1016/j.ajpath.2011.09.027)*

Regulatory T cells (T_{reg} cells) are a unique subset of T cells that play a critical role in maintaining immune tolerance.[1–3] The expression of the transcription factor forkhead box p3 (Foxp3) is the genetic hallmark of T_{reg} cells.[4–6] Foxp3-targeted genes in T_{reg} cells are up-regulated or down-regulated, suggesting that Foxp3 functions as both a transcriptional activator and a repressor.[7] Previous evidence indicates that Foxp3 controls T_{reg} functions by interacting with multiple transcription factors.[8] The function or expression of Foxp3 is controlled through complexes formed with other transcription factors, such as nuclear factor of activated T cells (NFAT), RUNX1/acute myelogenous leukemia (AML) 1, and nuclear factor kappa-B (NF-κB).[9,10] In addition, Foxp3 can maintain T_{reg} cell unresponsiveness (anergy) by selectively inhibiting the promoter DNA-binding activity of activator protein 1 (AP-1).[11] However, the molecular mechanism by which Foxp3 switches between transcriptional activation and repression in T_{reg} cells has not been well defined.

Previously, we reported autoimmune exocrinopathy in salivary and lacrimal glands resembling Sjögren's syndrome in C-C-chemokine receptor 7 (CCR7)-deficient ($Ccr7^{-/-}$) mice.[12] Enhanced immunity in $Ccr7^{-/-}$ mice is caused by defective lymph node (LN) positioning of T_{reg} cells and consequent impairment of suppressor function.[13] In a recent report, we demonstrated that CCR7 essentially governs the patrolling functions of T_{reg} cells by controlling their migration to target organs to maintain autoimmunity.[14] Furthermore, we found that the migratory function of $Ccr7^{-/-}$ T_{reg} cells in response to sphingosine 1-phosphate (S1P) was impaired, suggesting that CCR7

Supported by Funding Program for Next Generation World-Leading Researchers in Japan (LS090), Grants-in-Aid for Scientific Research (no. 17109016 and 17689049) from the Ministry of Education, Science, Sport, and Culture of Japan, and by funds from the Uehara Memorial Foundation and the Takeda Science Foundation (N.I.).

Accepted for publication September 13, 2011.

Supplemental material for this article can be found at *http://ajp.amjpathol.org* or at doi: 10.1016/j.ajpath.2011.09.027.

Address reprint requests to Naozumi Ishimaru, D.D.S., Ph.D., Department of Oral Molecular Pathology, Institute of Health Biosciences, The University of Tokushima Graduate School, 3-18-15 Kuramotocho, Tokushima 770-8504, Japan. E-mail: ishimaru@dent.tokusghima-u.ac.jp.

participates in the molecular mechanism underlying the migratory function of peripheral T_{reg} cells through S1P and one of its receptors, $S1P_1$.[14] In contrast, at the molecular level, T_{reg} cells in $S1P_1$-deficient mice were found to be defective in egress from the thymus; the number of peripheral T_{reg} cells in $S1P_1$-deficient mice was also increased, compared with peripheral T_{reg} cells in control mice.[15] Furthermore, $S1P_1$ transgenic mice developed autoimmune lesions because of a decrease in the number of T_{reg} cells in the thymus.[15] The S1P-$S1P_1$ axis is thus believed to play an important role in restraining the development and function of $Foxp3^+$ T_{reg} cells.

Mitogen-activated protein kinase (MAPK) signaling and AP-1 components are crucial in $S1P_1$ signaling in peripheral T cells.[16] In addition, the function of T_{reg} cells can be regulated by Foxp3 binding to phosphorylated c-Jun, thereby controlling AP-1 transcriptional activity.[11] Although the relationship between CCR7 and S1P/$S1P_1$ signaling in peripheral T_{reg} cells has not been clarified, it is possible that interactions among several molecules (including CCR7, S1P/$S1P_1$, and Foxp3) play a critical role in controlling the migratory response of peripheral T_{reg} cells.

In the present study, analysis of defective T_{reg} cells in *Ccr7*$^{-/-}$ mice revealed a novel regulation of Foxp3 nuclear localization that controls $S1P_1$-mediated AP-1 signaling after T_{reg} cell migration.

Materials and Methods

Mice

Ccr7$^{-/-}$, *Ccr7*$^{+/+}$ and C57BL/6 mice were reared in our specific pathogen-free mouse colony. Mice were provided food and water *ad libitum*. Experiments were humanely conducted under the regulation and permission of the Animal Care and Use Committee of the University of Tokushima (Tokushima, Japan).

Histological Analysis

All organs were removed from mice, fixed with 10% phosphate-buffered formaldehyde (pH 7.2), and prepared for histological examination. Sections were stained with H&E.

Cell Preparation

T_{reg} cells and $CD25^-CD4^+$ cells were enriched from LNs. In brief, $CD4^+$ cells were prepared using anti-B220, CD8, MHC class II, and NK1.1 monoclonal antibodies (mAbs) (eBioscience, San Diego, CA) and magnetic beads (Dynal Biotech, Oslo, Norway). $CD25^+CD4^+$ or $CD25^-CD4^+$ cells were enriched using biotin-conjugated anti-CD25 mAb, magnetic beads, and a CELLection biotin binder kit (Dynal Biotech) or a regulatory T cell isolation kit (Miltenyi Biotec, Auburn, CA). The enriched $CD25^+CD4^+$ cells were confirmed to be approximately 90% $Foxp3^+$.

In Vitro *Suppression Assay*

For suppression assays, a total of 5×10^4 $CD25^-CD4^+$ T cells from C57BL/6 mice were stimulated with plate-coated anti-CD3 mAb (0.5 μg/mL) for 72 hours together with 1.25, 2.5, and 5×10^4 $CD25^+CD4^+$ T cells from the LNs of wild-type (WT) and *Ccr7*$^{-/-}$ mice. [^{3}H]-Thymidine incorporation during the last 12 hours of the culture for 72 hours was evaluated using an automated liquid scintillation β counter (Hitachi Aloka Medical, Ltd., Tokyo, Japan).

ELISA

For detection of IL-4, IL-10, and TGF-β, $CD25^+CD4^+$ T cells were stimulated with plate-coated anti-CD3 mAb for 24 hours. The supernatants were added to microtiter plates precoated with an antibody specific for IL-4, IL-10, and TGF-β. The biotinylated antibody was added, and the plate was incubated for 2 hours at room temperature. After a wash, streptavidin-horseradish peroxidase solution was added to each well and the plate was incubated for 30 minutes. Finally, stabilized chromogen substrate was added to each well, and the absorbance of each well was read at 450 nm using an automated microplate reader (Bio-Rad Laboratories, Hercules, CA). Cytokine concentrations were obtained according to standard curves.

Confocal Microscopic Analysis

Cells were deposited onto poly-L-lysine-coated glass slides, and spun in a cytospin centrifuge. Sections were stained with 1 μg/mL of primary antibodies against phosphorylated ERK1/2, phosphorylated c-Jun (BD Biosciences, San Jose, CA), phosphorylated Rac-1 (Cell Signaling Technology, Danvers, MA), and Foxp3 (eBioscience, San Diego, CA) for 1 hour. After three washes in PBS, sections were stained with Alexa Fluor 568 donkey anti-rat IgG (H+L) (Molecular Probes; Invitrogen, Carlsbad, CA) or Alexa Fluor 488 horse anti-rabbit IgG (H+L) secondary antibodies for 30 minutes and washed with PBS. The nuclei were stained with DAPI. Sections were visualized with a laser scanning confocal microscope (Carl Zeiss MicroImaging, Göttingen, Germany). A 63×/1.4 oil differential interference contrast (DIC) objective lens was used. Quick Operation software, version 3.2 (Carl Zeiss), was used for image acquisition and Adobe Photoshop CS2 software (Adobe System, San Jose, CA) was used for image processing. Nuclear localization of Foxp3 and DAPI was evaluated within the imaging system.

Real-Time Quantitative RT-PCR

Total RNA was extracted from the T_{reg} cells of WT and *Ccr7*$^{-/-}$ mice with ISOGEN (Wako Pure Chemical, Osaka, Japan) and was then reverse-transcribed. Transcript levels of Gi, Rac-1, Foxp3, and β-actin were analyzed using the DNA engine OPTICOM system (Bio-Rad Laboratories) with SYBR Premix Ex Tag (Takara, Kyoto,

Japan). Primer sequences were as follows: Gi forward, 5′-TTTCTCTGGATGGGATGAGG-3′ and reverse, 5′-CCGAACCTCATGTTGTGTTG-3′; Rac-1 forward, 5′-GCCACTCAACGAGAGCCTAC-3′ and reverse, 5′-TCGGTTCTCCAGCTTGACTT-3′; Foxp3 forward, 5′-CCCAGGAAAGACAGCAACCTT-3′ and reverse, 5′-TTCTCACAACCAGGCCACTTG-3′; and β-actin forward, 5′-AAATCTGGCACCACACCTTC-3′ and reverse, 5′-GAGGCGTACAGGGATAGCA-3′.

Cell Culture and Migration Assay

For cell culturing with S1P or chemokines, cells were incubated in RPMI 1640 medium without fetal calf serum in the presence of S1P (0 to 100 nmol/L), CCL19 (100 ng/mL), or CCL21 (100 ng/mL) with plate-coated anti-CD3 mAb (0.5 μg/mL) for 3 to 12 hours. To evaluate chemotaxis by S1P, CCL19, or CCL21 in the T_{reg} cells of WT and *Ccr7*$^{-/-}$ mice, a Cultrex 96-well cell migration assay kit (Trevigen, Gaithersburg, MD) was used according to the manufacturer's instructions. Before the assay, the cells were starved for 24 hours in serum-free medium and incubated in RPMI 1640 without fetal calf serum. In addition, the cells were pretreated with inhibitors, including FTY720 (BioVision, San Francisco, CA), PTX, rapamycin, SB203580, and PD98059 (Sigma-Aldrich, St. Louis, MO) for 6 to 12 hours, and then the migration assay was performed.

Western Blotting and Immunoprecipitation

Whole-cell extracts of T_{reg} cells were prepared using a Pierce M-PER mammalian protein extraction kit (Thermo Fisher Scientific, Rockford, IL) or nuclear/cytosol fraction kit (BioVision). A total of 10 μg of each sample per well was applied to each well and was electrophoresed on 10% SDS-PAGE. Thereafter, the protein was electrophoretically transferred onto polyvinylidene difluoride membranes. Blocked membranes were incubated with antibodies specific for $S1P_1$ (Cayman Chemical, Ann Arbor, MI), Rac-1, phosphorylated Rac-1 (Cell Signaling Technology), Gi (Millipore-Chemicon International, Temecula, CA), phospho-c-Jun (BD Biosciences), total c-Jun (BD Biosciences), or glyceraldehyde-3-phosphate dehydrogenase (GAPDH; Santa Cruz Biotechnology, Santa Cruz, CA). Horseradish peroxidase-conjugated rabbit or mouse IgG was used as the secondary antibody. Protein binding was visualized using Amersham ECL Western blotting detection reagents (GE Healthcare, Piscataway, NJ). To quantify protein expression, the chemiluminescence image was analyzed using a ChemiDoc XRS system (Bio-Rad Laboratories). For immunoprecipitation, purified proteins captured with anti-Foxp3 mAb were incubated with Dynabeads protein G (Invitrogen). To remove genomic DNA, proteins were treated with DNase I. Precipitated proteins were analyzed by immunoblotting with anti-c-Jun or anti-Foxp3 (e-Bioscience) antibody.

c-Jun Transcriptional Activity

The transcriptional activity of c-Jun in the nuclear extracts from T_{reg} of WT and *Ccr7*$^{-/-}$ mice was analyzed using an Upstate c-Jun transcription factor assay kit (Millipore, Billerica, MA). In brief, nuclear extracts were incubated with a biotinylated double-stranded oligonucleotide probe containing the consensus sequence for c-Jun on a streptavidin-coated plate. Captured complexes were incubated with c-Jun antibody, horseradish peroxidase-conjugated secondary antibody, and tetramethylbenzidine substrate. The absorbance of samples was measured using an automated microplate reader at 450 nm.

Statistical Analysis

Student's *t*-test was used for statistical analysis. A *P* value of <0.05 was considered statistically significant.

Results

Relationship between Autoimmune Lesions and T_{reg} Cells in Ccr7$^{-/-}$ Mice

We found a significantly reduced proportion of Foxp3$^+$ T_{reg} cells in target organs, including the salivary and lacrimal glands, of *Ccr7*$^{-/-}$ mice, compared with *Ccr7*$^{+/+}$ mice, at approximately 3 months of age. This led to significantly increased retention of T_{reg} cells in the LNs of *Ccr7*$^{-/-}$ mice until mice were 6 months of age.[14] However, it is unclear whether the proportion of T_{reg} cells in target organs and LNs changed with aging during these 6 months. More severe autoimmune lesions in lacrimal glands of *Ccr7*$^{-/-}$ mice were observed at 9 and 18 months of age (Figure 1A). At 18 months of age, extensive infiltration of lymphocytes with destruction of exocrine gland cells was detected in *Ccr7*$^{-/-}$ mice (Figure 1A). The proportion of Foxp3$^+$ CD4$^+$ T_{reg} cells in the cervical LNs of *Ccr7*$^{-/-}$ mice was significantly increased, compared with WT mice, until 18 months of age (Figure 1B). The retention of T_{reg} cells in the LNs of *Ccr7*$^{-/-}$ mice increased with aging. In contrast, the proportion of T_{reg} cells in lacrimal glands of *Ccr7*$^{-/-}$ mice was significantly reduced, compared with *Ccr7*$^{+/+}$ mice (Figure 1C). In addition, although the absolute number of T_{reg} cells in the cervical LNs of normal mice decreased with aging, the number of LN T_{reg} cells in *Ccr7*$^{-/-}$ mice increased (Figure 1D). At 3 and 9 months of age, the cell number in T_{reg} cells in *Ccr7*$^{-/-}$ mice was significantly reduced, compared with control mice (Figure 1D). At 18 months of age, the number of cells of *Ccr7*$^{-/-}$ mice was similar to that of control mice (Figure 1D). Given that the total cell number in the LNs of *Ccr7*$^{-/-}$ mice significantly decreased, compared with control mice, the proportion of T_{reg} cells from *Ccr7*$^{-/-}$ mice was higher than that from control mice (Figure 1B). In contrast, the number of T_{reg} cells in lacrimal glands of *Ccr7*$^{-/-}$ mice were significantly reduced, compared with control mice (Figure 1E). These findings are consistent with our previous report that Foxp3$^+$ CD4$^+$

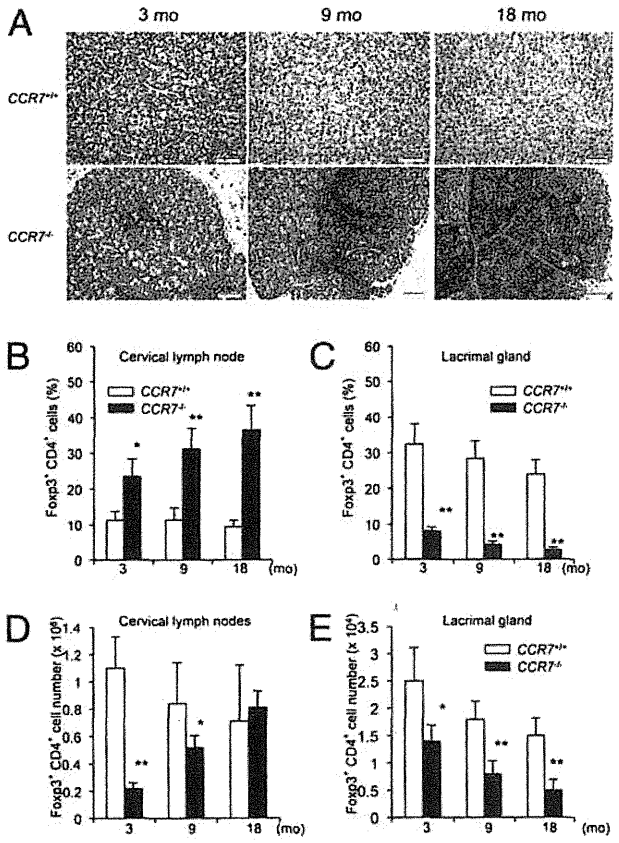

Figure 1. Autoimmune exocrinopathy and T_{reg} cell in *Ccr7*$^{-/-}$ mice. **A:** Histology of lacrimal glands of *Ccr7*$^{+/+}$ and *Ccr7*$^{-/-}$ mice at 3, 9, and 18 months of age. H&E staining was performed on paraffin-embedded sections. Images are representative of 5 to 7 mice per group. Scale bars = 500 μm. **B:** The proportions of Foxp3$^+$ CD4$^+$ T_{reg} cells in cervical LNs in *Ccr7*$^{+/+}$ and *Ccr7*$^{-/-}$ mice at 3, 9, and 18 months of age were detected by flow cytometric analysis. **C:** The proportions of Foxp3$^+$ CD4$^+$ T_{reg} cells in lacrimal glands of *Ccr7*$^{+/+}$ and *Ccr7*$^{-/-}$ mice at 3, 9, and 18 months of age were detected by flow cytometric analysis. **D:** Quantification of Foxp3$^+$ CD4$^+$ T_{reg} cells in cervical LNs of *Ccr7*$^{+/+}$ and *Ccr7*$^{-/-}$ mice at 3, 9, and 18 months of age. **E:** Quantification of Foxp3$^+$ CD4$^+$ T_{reg} cells in lacrimal glands of *Ccr7*$^{+/+}$ and *Ccr7*$^{-/-}$ mice at 3, 9, and 18 months of age. Results are presented as means ± SD for five mice in each group. $^*P < 0.05$; $^{**}P < 0.005$ versus WT.

T_{reg} cell numbers are significantly reduced in target organs, such as salivary or lacrimal glands, in *Ccr7*$^{-/-}$ mice and in patients with Sjögren's syndrome.[14]

Chemotactic Response to S1P and Suppressive Function of Ccr7$^{-/-}$ *T*$_{reg}$ *Cells*

We examined in *vitro* chemotactic responses of CD4$^+$ T cells from WT and *Ccr7*$^{-/-}$ mice in response to S1P. In both WT and *Ccr7*$^{-/-}$ mice, no migratory responses of CD25$^+$CD4$^+$ T_{reg} cells were observed with the addition of S1P (Figure 2A). Although there was a small increase in the chemotactic response of WT and *Ccr7*$^{-/-}$ CD25$^-$CD4$^+$ T cells to S1P, there were no differences in the response between WT and *Ccr7*$^{-/-}$ mice (Figure 2B). Next, we examined the chemotactic response of anti-CD3 mAb-engaged *Ccr7*$^{-/-}$ CD4$^+$ cells to S1P, and found that the migratory response of *Ccr7*$^{-/-}$ T_{reg} cells to S1P was significantly impaired, compared with WT T_{reg} cells (Figure 2C). In contrast, the response of CD25$^-$CD4$^+$ cells of *Ccr7*$^{-/-}$ mice was not impaired (Figure 2D). These findings suggest that the chemotactic response of T cells to S1P is dependent on T-cell receptor/CD3 signaling.

To determine whether there were migratory responses to chemoattractants other than S1P, we performed migration assays using IL-6 and MIP-2, and found no difference in the migration activity between WT and *CCR7*$^{-/-}$ T_{reg} cells. The results for anti-CD3 mAb-engaged T_{reg} cells are shown in Figure 2, E and F. Moreover, there were also no differences in migration activity in response to IL-6 and MIP-2 between unstimulated WT and *CCR7*$^{-/-}$ T_{reg} cells (data not shown). In contrast, when we examined the *in vitro* suppressive function of *Ccr7*$^{-/-}$ T_{reg} cells, we found that the suppression of *Ccr7*$^{-/-}$ T_{reg} cells on the proliferative response elicited by the anti-CD3 mAb in normal CD25$^-$CD4$^+$ cells from C57BL/6 mice was similar to that of WT T_{reg} cells (Figure 2G). In addition, there were no differences in the production of suppressive cytokines such as IL-4, IL-10, or TGF-β in *Ccr7*$^{-/-}$ or WT T_{reg} cells (Figure 2H). These findings suggest that CCR7 signaling controls the migration of T_{reg} cells, but does not control the suppressive function of T_{reg} cells. This is consistent with the failure of *in vivo* migration to target organs in *Ccr7*$^{-/-}$ T_{reg} cells.[14]

Activation of Signaling Molecules Downstream of S1P$_1$ *in* Ccr7$^{-/-}$ *T*$_{reg}$ *Cells*

$S1P_1$, one of receptors for S1P, is expressed on the cell surface and is known to be internalized when the S1P ligand binds to $S1P_1$ after activation of the signaling molecules required for the migratory response.[17] We detected expression of $S1P_1$ in WT and *Ccr7*$^{-/-}$ T_{reg} cells by Western blotting with anti-$S1P_1$ polyclonal antibodies. There was no difference in $S1P_1$ expression between WT and *Ccr7*$^{-/-}$ T_{reg} cells (Figure 3, A and B). $S1P_1$ has been shown to signal exclusively through the heterotrimeric G protein Gi.[18] We therefore used Western blotting to evaluate Gi expression in WT and *Ccr7*$^{-/-}$ T_{reg} cells after anti-CD3 mAb and S1P treatment (see Supplemental Figure S1A at *http://ajp.amjpathol.org*). There were no differences in expression between WT and *Ccr7*$^{-/-}$ T_{reg} cells, and this was unchanged by stimulus (see Supplemental Figure S1A at *http://ajp.amjpathol.org*).

The phosphorylation of Rac-1,[19] a key molecule downstream of G-protein signaling, was observed in WT T_{reg} cells but not in *Ccr7*$^{-/-}$ T_{reg} cells stimulated with the anti-CD3 mAb and S1P (Figure 3C). Phosphorylation of Rac-1 was evaluated by Western blotting. The phosphorylation of Rac-1 in WT T_{reg} cells was detectable after CD3 engagement, and the addition of S1P enhanced Rac-1 phosphorylation in anti-CD3 mAb-stimulated T_{reg} cells (Figure 3D). In contrast, the phosphorylation of Rac-1 in *Ccr7*$^{-/-}$ T_{reg} cells was low, compared with that in WT T_{reg} cells (Figure 3D). In contrast, there was no difference in Rac-1 phosphorylation between WT and *Ccr7*$^{-/-}$ CD25$^-$CD4$^+$ T cells (see Supplemental Figure S2 at *http://ajp.amjpathol.org*). These findings demonstrate the impairment of the signaling pathway in *Ccr7*$^{-/-}$ T_{reg} cells.

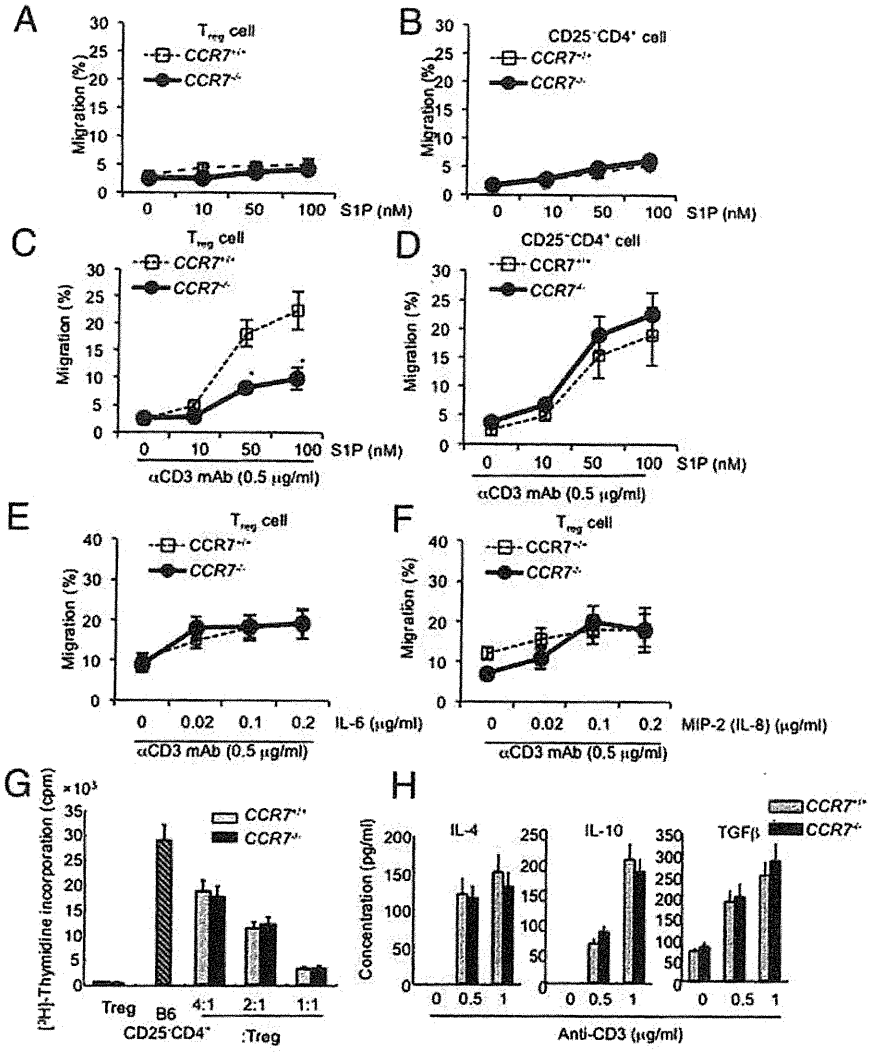

Figure 2. Signaling pathway in *Ccr7*$^{-/-}$ T_{reg} cells. **A** and **B:** Migration assay of T_{reg} cells (**A**) and $CD25^-CD4^+$ T cells (**B**) from LNs of WT and *Ccr7*$^{-/-}$ mice in response to S1P (0 to 100 nmol/L) was performed using purified T_{reg} and $CD25^-CD4^+$ T cells for 12 hours. **C** and **D:** Migration assay of T_{reg} cells (**C**) and $CD25^-CD4^+$ T cells (**D**) from LNs of WT and *Ccr7*$^{-/-}$ mice in response to S1P (0 to 100 nmol/L) was performed using anti-CD3mAb-stimulated T cells for 12 hours. **E:** Migratory response to IL-6 (0 to 0.2 μg/mL) in anti-CD3 mAb-stimulated T_{reg} cells. **F:** Migratory response to MIP-2 (0 to 0.2 μg/mL) in anti-CD3 mAb-stimulated T_{reg} cells. Data are presented as means ± SD (n = 3) and are representative of three independent experiments. **G:** *In vitro* suppression assays were performed by evaluation of the proliferative response in purified $CD25^-CD4^+$ T cells from C57BL/6 mice. $CD25^-CD4^+$ T cells were cocultured with WT or *Ccr7*$^{-/-}$ T_{reg} cells on anti-CD3 mAb-coated plates for 72 hours. The proliferative response was evaluated by incorporation of $[^3H]$-thymidine during the last 18 hours of incubation. Data are presented as means ± SD (n = 3) and are representative of three independent experiments. **H:** WT or *Ccr7*$^{-/-}$ T_{reg} cells were stimulated with anti-CD3 mAb for 24 hours. Concentrations of IL-4, IL-10, and TGF-β in the culture supernatants were measured by enzyme-linked immunosorbent assay. Data are presented as means ± SD (n = 3) and are representative of two independent experiments.

Next, we focused on examining migratory function and CCR7 signaling using a Gi protein inhibitor, pertussis toxin (PTX), and an S1P receptor agonist, FTY720 (Figure 3E). The increased migratory response of WT T_{reg} cells on stimulation with anti-CD3 mAb and S1P was reduced by pretreatment with FTY720 or PTX (Figure 3E). Moreover, when WT T_{reg} cells were incubated with a CCR7 ligand (either CCL19 or CCL21) in addition to anti-CD3 mAb and S1P, migratory responses were significantly enhanced in contrast to the response to anti-CD3 mAb and S1P (Figure 3E). These enhanced responses were reduced with pretreatment of FTY720 and PTX to the levels of *Ccr7*$^{-/-}$ T_{reg} cells (Figure 3E). This result suggests that CCR7 signaling in T_{reg} cells is dependent on cooperation with S1P/$S1P_1$ and Gi, in addition to CD3 signaling.

MAPK Signaling in Ccr7$^{-/-}$ *T_{reg} Cells*

To further elucidate the importance of $S1P_1$ signaling for T_{reg} cell egress, we analyzed MAPK signaling and the AP-1 components that play crucial roles in $S1P_1$ signaling in T cells.[16] Phosphorylation of ERK after stimulation with anti-CD3 mAb and S1P was observed in WT T_{reg} cells, but not in *Ccr7*$^{-/-}$ T_{reg} cells (Figure 4A), and this phosphorylation was enhanced with addition of S1P (Figure 4B). To determine whether this signaling was through MAPK or Akt-mTOR, we performed migration assays using the mTOR inhibitor rapamycin and two MAPK inhibitors. The migratory activity of WT T_{reg} cells increased with treatment of anti-CD3 mAb and S1P, and was not fully inhibited by pretreatment with rapamycin (Figure 4C). The increased migratory response of WT T_{reg} cells was significantly inhibited by the addition of the ERK MAPK inhibitor PD98059, but not by the addition of the p38 MAPK inhibitor SB203580 (Figure 4C). These findings suggest that CCR7-mediated ERK activation plays a crucial role in the migratory function of T_{reg} cells.

Association of c-Jun Activity with CCR7/$S1P_1$ Signaling

When T_{reg} cells of WT mice were stimulated with anti-CD3 mAb and S1P, phosphorylated c-Jun protein colocalized with Foxp3 in the nucleus. In contrast, phosphorylation of c-Jun was undetectable in *Ccr7*$^{-/-}$ T_{reg} cells stimulated